

Experimental and Theoretical Studies of Magnetic Exchange in Silole-Bridged Diradicals

Nans Roques,^[a] Philippe Gerbier,^{*[a]} Ulrich Schatzschneider,^[b] Jean-Pascal Sutter,^[c, f] Philippe Guionneau,^[c] José Vidal-Gancedo,^[d] Jaume Veciana,^[d] Eva Rentschler,^[e] and Christian Guérin^[a]

Abstract: Five bis(*tert*-butylnitroxide) diradicals connected by a silole (**7a–d**) or a thiophene (**12**) ring as a coupler were studied. Compound **12** crystallizes in the orthorhombic space group *Pna*2₁ with *a* = 20.752(5), *b* = 5.826(5), and *c* = 34.309(5) Å. X-ray crystal structure determination, electronic spectroscopy, variable-temperature EPR spectroscopy, SQUID measurements and DFT computations (UB3LYP/6-31+G*) were used to study the molecular conformations and electronic spin coupling in this series of molecules. Whereas compounds **7b**, **7c**, and **7d** are quite stable both in solution and in the solid state, **7a** and **12** undergo a partial electronic rearrangement to both a diamagnetic quinonoidal form and a monoradical species owing to the fact that they correspond to the open form of a π -conjugated Kekulé struc-

ture. In the solid state, magnetic measurements indicate that the diradicals are all antiferromagnetically coupled, as expected from their topology. These interactions are best reproduced by means of a “Bleaney–Bowers” model that gives values of $J = -142.0 \text{ cm}^{-1}$ for **7a**, -1.8 cm^{-1} for **7b**, -1.3 cm^{-1} for **7c**, -4.2 cm^{-1} for **7d**, and -248.0 cm^{-1} for **12**. The temperature dependence of the EPR half-field transition in frozen dichloromethane solutions is consistent with singlet ground states and thermally accessible triplet states for diradicals **7b**, **7c**, and **7d** with ΔE_{T-S} values of 3.48, 2.09, and 8 cm^{-1} , respectively. No

Keywords: density functional calculations • EPR spectroscopy • magnetic interactions • nitroxide diradicals • siloles

evidence of a populated triplet state was found for diradicals **7a** and **12**. Similarities between the ΔE_{T-S} and J values ($\Delta E_{T-S} = -2J$) clearly show the intramolecular origin of the observed antiferromagnetic interaction. Analyses of the data with a “Karplus–Conroy”-type equation enabled us to establish that the silole ring, as a whole, allows a more efficient magnetic coupling of the two nitroxide radicals attached to its 2,5-positions than the thiophene ring. This superiority probably originates from the nonaromaticity of the silole which thus permits a better magnetic interaction through it. DFT calculations also support the experimental results, indicating that the magnetic exchange pathway preferentially involves the carbon π system of the silole.

[a] Dr. N. Roques, Dr. P. Gerbier, Prof. C. Guérin
Laboratoire de Chimie Moléculaire et Organisation du Solide
Université Montpellier 2, C.C.007
Place E. Bataillon, 34095 Montpellier Cedex 5 (France)
Fax: (+33)467-143-852
E-mail: gerbier@univ-montp2.fr


[b] Dr. U. Schatzschneider
Institut für Pharmazie und Molekulare Biotechnologie
Abteilung Chemie, Ruprecht-Karls-Universität Heidelberg
Im Neuenheimer Feld 364, 69120 Heidelberg (Germany)

[c] Dr. J.-P. Sutter, Dr. P. Guionneau
Institut de Chimie de la Matière Condensée de Bordeaux
CNRS UPR 9048, Université Bordeaux 1
87, Av. Dr. Schweitzer, 33608 Pessac (France)

[d] Dr. J. Vidal-Gancedo, Prof. J. Veciana
Institut de Ciència de Materials de Barcelona - CSIC, Campus de la
UAB, 08193 Bellaterra (Spain)

[e] Prof. E. Rentschler
Institut für Anorganische Chemie und Analytische Chemie
Johannes-Gutenberg-Universität Mainz
Duesbergweg 10–14, 55128 Mainz (Germany)

[f] Dr. J.-P. Sutter
Present address: Laboratoire de Chimie de Coordination du CNRS
Université Paul Sabatier, 205 route de Narbonne
31077 Toulouse (France)

 Supporting information for this article is available on the WWW under <http://www.chemeurj.org/> or from the author. It includes UB3LYP/6-31G-optimized geometries for radicals **7a–d**, CIF file and crystal packing of **12** in the *ac* plane, selected bond lengths for selected benzenoid and quinonoid structures, bond length variations in 2,5-diphenylthiophenes and *p*-terphenylquinones for the adjacent phenyl ring and the central thiophene ring.

Introduction

Organosilicon-based molecules have attracted much attention because of their unique optoelectronic properties and their importance in applications such as photoresists, photoconductors, nonlinear optical materials, and light-emitting devices.^[1–4] Such interesting properties mainly originate from the unusual types of conjugation that are encountered in polysilanes ($\sigma(\text{SiSi})$ -type),^[5] in compounds in which oligosilanylene units are alternating with carbon π systems ($\sigma(\text{SiSi})$ - π type, Figure 1 b),^[6] and in compounds in which sila-

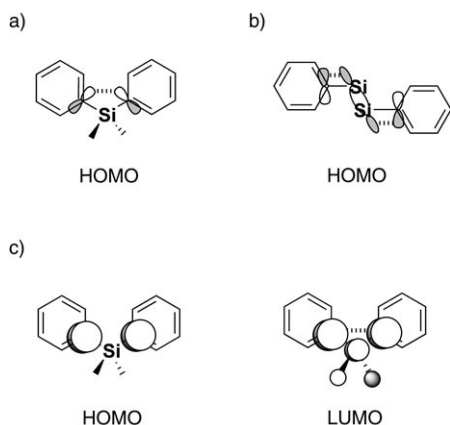


Figure 1. Different types of conjugation between two aromatic rings through organosilicon units. a) Through-space overlap of the aromatic π orbitals in the butterfly-shaped diarylsilane family. b) $\sigma(\text{SiSi})$ - π conjugation in the diaryldisilane family. c) $\sigma^*(\text{Si})$ - π^* conjugation in the planar diarylsilane family.

nylene units are alternating with carbon π systems ($\sigma^*(\text{Si})$ - π^* type, Figure 1 c).^[7] In general, the attachment of a silicon atom to a π system is not an innocent act since its presence induces appreciable electronic perturbations, which have been exploited by organic chemists for a long time. Among others, the Birch reduction of aromatic rings may be adequately directed by organosilicon substituents since they stabilize transient radical anions on the carbon atom to which they are bound.^[8]

Another interesting example of the electronic perturbation induced by the presence of a silicon atom is found in five-membered heteropentacycles: while furan ($X = \text{O}$), pyrrole ($X = \text{NR}$), and thiophene ($X = \text{S}$) derivatives are colorless, silacyclopentadiene or silole ($X = \text{SiR}_2$) derivatives are highly colored compounds because of the lowest HOMO–LUMO gap of the series. This characteristic originates from an unusual low-lying LUMO level associated with σ^* - π^* conjugation (Figure 1 c) arising from the interaction between the σ^* orbital of the two exocyclic σ bonds on the silicon atom and the π^* orbital of the butadiene moiety, as exemplified in Figure 2 for 2,3,4,5-tetraphenyl-1,1-dimethylsilole (**1**).^[7] Consequently, siloles have a high electron affinity and the fast electron mobility makes them molecules

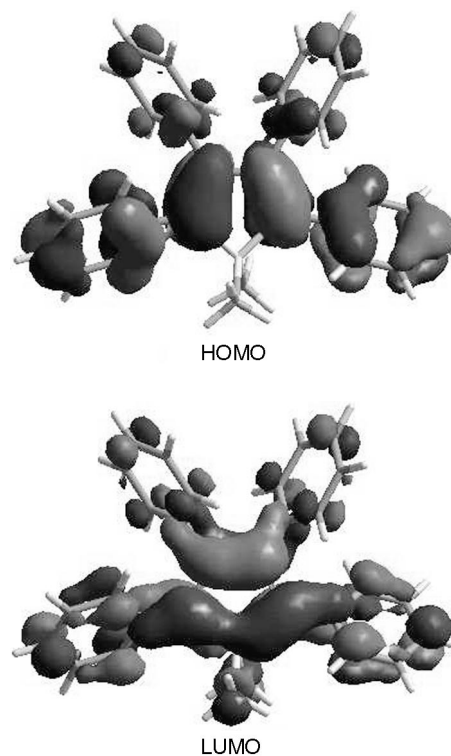
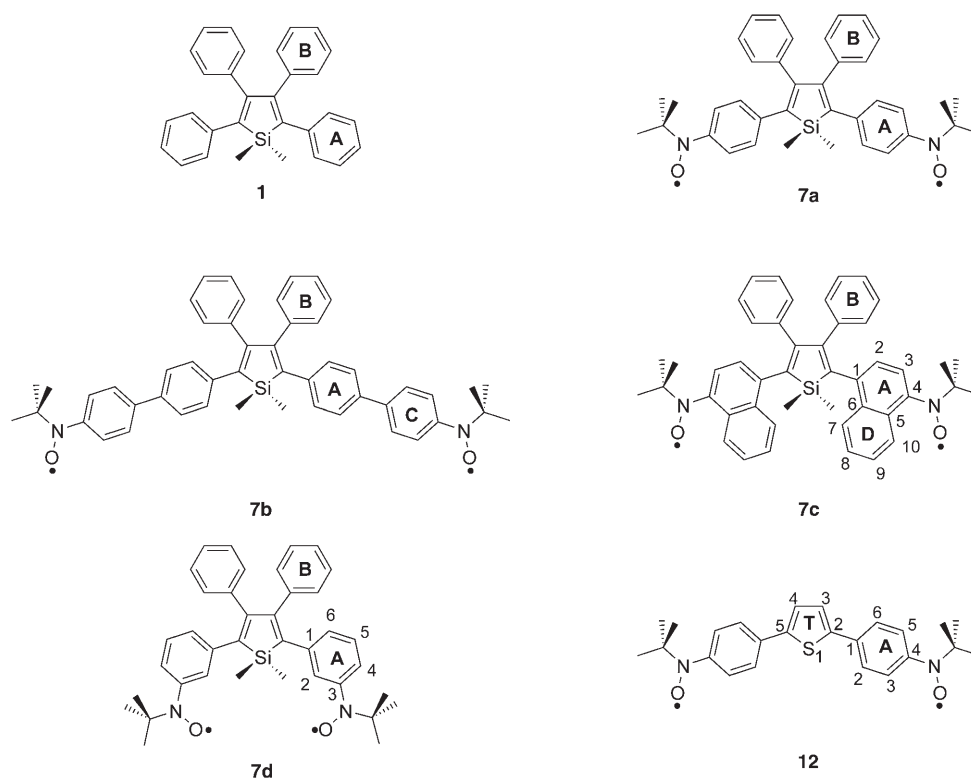


Figure 2. HOMO and LUMO orbitals (6-31G* level) of 2,3,4,5-tetraphenyl-1,1-dimethylsilole (**1**) showing the σ^* - π^* conjugation in the excited state.

of choice to build highly efficient light-emitting layers for electroluminescent devices.^[2,9–12]

Bearing in mind the remarkable properties of silicon-containing molecules, several works in the field of molecular magnetism have been devoted to the syntheses and characterization of model compounds based on paramagnetic centers (organic radicals or paramagnetic metal ions) linked by organosilicon units.^[3,9,13–20] The connection of spin-bearing moieties through silicon-containing units was achieved in such a way that the magnetic interaction may take place through the molecular skeleton via the set of conjugated bonds available in such systems following two different approaches involving either the use of silanylene or disilanylene units as spin couplers. These studies revealed that 1) the silicon atom, when it is part of a single pathway spacer, can act as a magnetic coupler, 2) as in other heteroatom-containing couplers, the nature of the magnetic exchange depends on the connectivity of the paramagnetic centers, and finally 3) the strength of the magnetic interaction strongly depends on the orbital overlap between the silanylene or disilanylene coupler and the spin-bearing π systems. However, while several studies of systems with paramagnetic centers connected through the 2,5-positions of heteropentacycles, such as thiophene, pyrrole or furan, have been reported, none of them were dedicated to siloles until we briefly described the synthesis and properties of the silole-based diradical **7d** (Scheme 1) in a preliminary communication. Our objectives were: 1) to study the silole as a



Scheme 1. Silole- and thiophene-bridged diradicals.

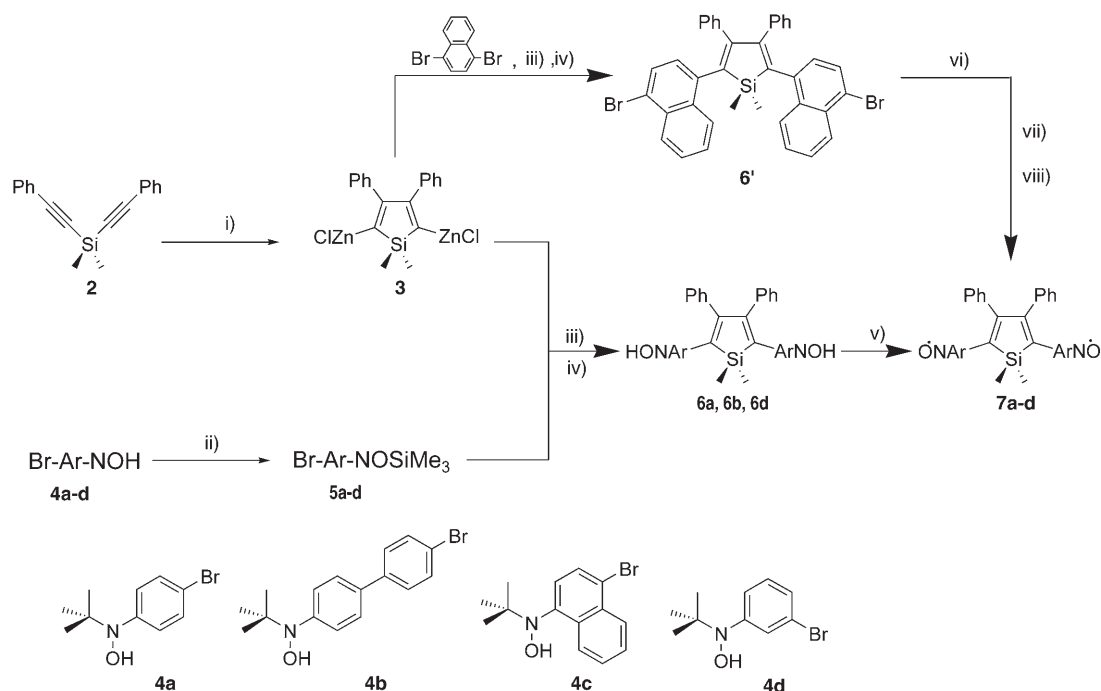
magnetic coupler, to determine what kind of magnetic interaction is mediated through it, and the role of the silicon atom in the magnetic exchange when it is incorporated into such a kind of ring; 2) to study the photoexcited state of the silole coupler, and 3) to try to use it as an access to photoexcited high-spin states following the strategy described by Teki et al. in the case of the anthracene coupler.^[21–23] Compound **7d**, which belongs to the pseudo-disjoint diradical class, allowed us to partially address the last two points: the silole coupler possesses a photoexcited triplet state, but the diradical did not show any high-spin photoexcited state.^[24] However, the very weak intramolecular antiferromagnetic interaction observed in this compound, mainly originating from its doubly disjoint character, prevented us from clearly determining whether the silole ring mediates magnetic interactions and whether the magnetic exchange pathway involves the silicon atom or not since the spin-density delocalization on the silole ring is very low in these systems.

To complete the study of the silole ring as a magnetic relay and to determine the role of the silicon atom in the magnetic exchange in such a five-membered coupler, we present herein a series of diradicals incorporating either the silole or the thiophene ring as a coupler, in which the relative position of the nitroxide radicals on the pendant aryl substituents (*para* versus *meta*, Scheme 1) has been changed to increase the spin density on the silole bridge. The synthesis as well as the structural and electronic characterization of this series of diradicals is presented here in detail. Their magnetic behavior has been investigated both in the solid

state and in dilute solutions, and the experimental data has been complemented by DFT calculations to shed some light on magnetic interactions mediated by this peculiar silicon-containing organometallic unit.

Results and Discussion

Synthesis: 2,5-Diaryl-3,4-diphenylsiloles were prepared as outlined in Scheme 2 by an adaptation of the general procedure described by Tamao and Yamaguchi.^[2,25] It involves the intramolecular reductive cyclization of bis(phenylethynyl)dimethylsilane (**2**) followed by a Pd-catalyzed crosscoupling reaction^[26,27] between organozinc derivative **3** and an adequately functionalized aryl bromide. The arylhydroxylamines **4a–d** were synthesized by a stepwise procedure starting from aryl dibromides that were first monolithiated with *n*-butyllithium at low temperature and then treated with 2-methyl-2-nitrosopropane.^[28,29] Because the following step involves reagent **3**, which is sensitive to the slightly acidic NOH groups, all hydroxylamine derivatives had to be protected with trimethylsilyl (TMS) groups, giving compounds **5a–d**, before they could be used in the reaction. The TMS protecting group was chosen because it is easily removed during the hydrolysis step without the need to use a nucleophilic agent that might lead to unwanted ring-opening reactions of the silole ring. The subsequent Pd-catalyzed cross-coupling reaction between **3** and **5a–d** followed by hydrolysis afforded bishydroxylamines **6a,b**, and **d** in good yields.

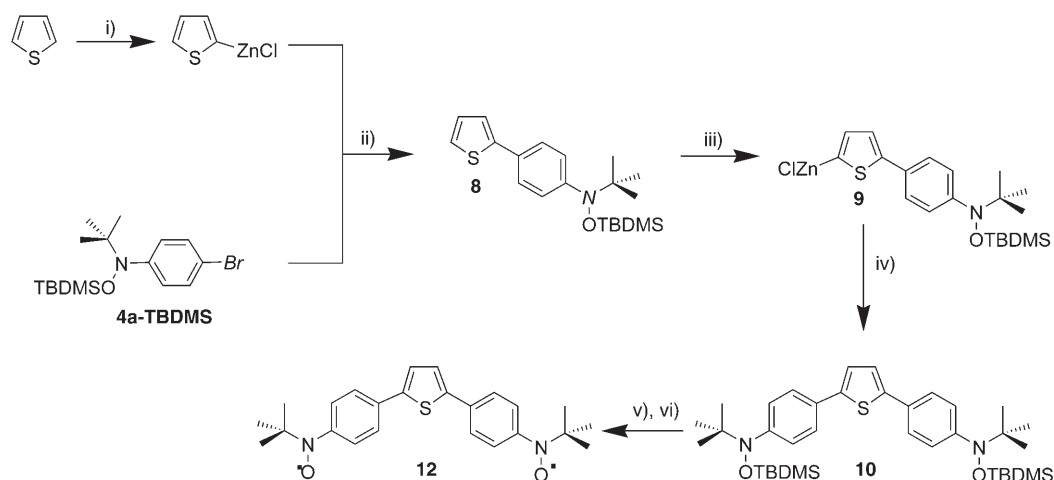


Scheme 2. i) 4 equiv Np/Li , THF; 4 equiv $[\text{ZnCl}_2(\text{tmeda})]$; ii) 3 equiv Me_3SiCl , 3 equiv Et_3N , THF; iii) $[\text{PdCl}_2(\text{PPh}_3)_2]$, THF; iv) 0.1 M HCl; v) Ag_2O , CH_2Cl_2 ; vi) TMEDA, $n\text{BuLi}$, $t\text{BuNO}$, Et_2O ; vii) 0.1 M HCl; viii) Ag_2O , CH_2Cl_2 .

Unfortunately, owing to its low stability, bishydroxylamine **6c** could not be obtained under such synthetic conditions. The silole derivatives **6a**, **b**, and **d** were further oxidized to the corresponding *tert*-butylnitroxide and nitronyl nitroxide diradicals with freshly prepared silver oxide as the oxidizing agent. As mentioned above, the low stability of **6c** forced us to synthesize diradical **7c** by a slightly different approach that involved the coupling reaction of **3** with excess dibromonaphthalene (to avoid the formation of silole-naphthalene oligomers) to afford dibromosilole **6'**. Compound **7c** was obtained in good yields from a one-pot reaction that included lithiation, intermediate formation of the bishydroxyl-

amine, and oxidation. The crude nitroxides were all purified over aluminum oxide or silica gel.

Compound **12** was synthesized and studied as a model compound for comparison. The synthesis of symmetrically disubstituted thiophene-bridged diradicals followed an adaptation of the procedure previously described by Takahashi et al. This involves the successive Pd-catalyzed crosscoupling reaction of aryl bromides with thienylzinc chloride.^[30] As outlined in Scheme 3 for diradical **12**, the first step involves the cross-coupling reaction of thienylzinc chloride with the *tert*-butyldimethylsilyl (TBDMS)-protected *N*-(4-bromophenyl)-*N*-*tert*-butylhydroxylamine (**4a-TBDMS**) to afford **8** in



Scheme 3. i) $n\text{BuLi}$, THF; ZnCl_2 ; ii) **4a-TBDMS**, $[\text{PdCl}_2(\text{PPh}_3)_2]$, THF; iii) $n\text{BuLi}$, THF; $[\text{ZnCl}_2(\text{tmeda})]$; iv) **4a-TBDMS**, $[\text{PdCl}_2(\text{PPh}_3)_2]$, THF; v) aq. HF, THF; vi) PbO_2 , CH_2Cl_2 .

73% yield. Organozinc chloride **9**, prepared from lithiated **8** and ZnCl_2 , was allowed to react with **4a-TBDMS** as in the first step to give **10** in 33% yield. Removal of the protecting TBDMS with HF in aqueous THF quantitatively yielded bishydroxylamine **11**, which was subsequently oxidized with lead dioxide in dichloromethane to afford diradical **12** as black needle-shaped crystals upon evaporation of the solvent with a 67% yield.

Geometries of the silole-bridged diradicals 7a–d: The determination of the conformational preferences of these diradicals is of utmost importance for the understanding of their magnetic behavior. Because crystals suitable for an X-ray structure determination could only be obtained for **7d** (Figure 3a),^[19] we turned to density functional theory (DFT) cal-

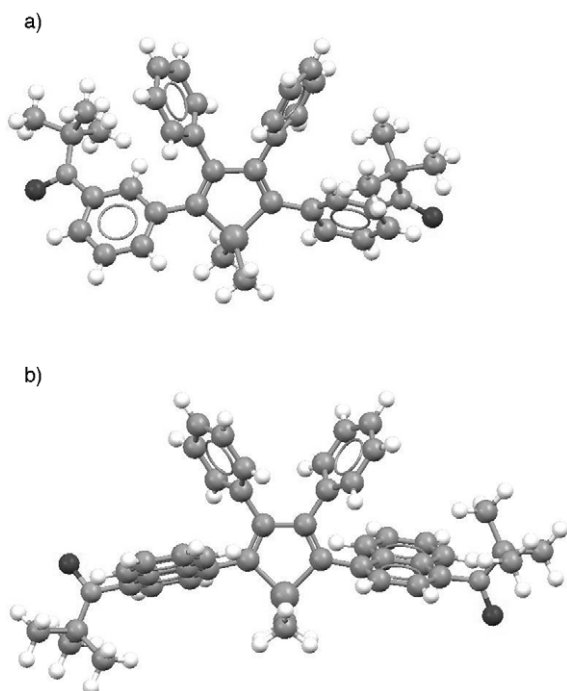


Figure 3. a) X-ray structure of **7d**. b) Optimized UB3LYP/6-31G geometry of **7c**.

culations with the UB3LYP functional to obtain information about the molecular conformations for the rest of the diradicals.^[31–33] Owing to the size of the molecules, geometry optimizations without symmetry constraints were performed with the 6-31G basis set to the standard convergence criteria as implemented in Gaussian 98.^[34] Such calculations were followed by single-point runs using a 6-31+G* basis with tight convergence and the ultrafine integration grid to obtain accurate energies and spin densities. Structurally characterized silole-bridged diradical **7d** served as a benchmark to test how well the experimentally determined geometry is reproduced by the calculations. Some relevant bond lengths, angles, and torsion angles are collected in Table 1 and are also compared to the mean values for the core SiC_4 ring of

Table 1. Selected bond lengths [\AA], angles and torsion angles [$^\circ$] for **7d**.

	X-ray structure	Optimized geometry	CSD data ^[a]
N–O	1.283	1.324	–
N–C(CH ₃) ₃	1.500	1.522	–
N–Ph ^{A[B]}	1.418	1.428	–
C–C in Ph ^A	1.366 to 1.397	1.392 to 1.412	–
Ph ^A –silole	1.480	1.480	–
C–C in Ph ^B	1.362 to 1.391	1.398 to 1.409	–
Ph ^B –silole	1.498	1.494	–
Si–CH ₃	1.854	1.916	1.869
Si–C2/C5	1.873	1.914	1.876
C=C	1.354	1.369	1.358
C–C	1.501	1.520	1.497
Ph ^B –C=C–Ph ^B	8.8	2.0	–
Ph ^A –C–C–Ph ^B	4.2	6.0	–
Ph ^A –C–Si–CH ₃	50.9 and –74.2	54.9 and –71.9	–
C–C=C	116.0	116.1	–
C=C–Si	107.9	108.4	–
CH ₃ –Si–CH ₃	108.4	109.8	–
CH ₃ –Si–C2/C5	109.7 and 118.4	109.8 and 111.5	–
Ph ^A –N–C(CH ₃) ₃	126.5	126.5	–
Ph ^A –N–O	116.2	116.7	–
C(CH ₃) ₃ –N–O	117.3	116.8	–
silole–Ph ^A	47.2	53.2	–
silole–Ph ^B	60.4	55.7	–
(CH ₃ –Si–CH ₃)–silole	82.5	85.9	–
Ph ^A –(CNO)	17.0	14.3	–

[a] Average data for 14 independent molecules in 12 structures, only structures not containing coordinated transition metals were considered. [b] See Scheme 1 for the labeling of the aromatic rings.

other purely organic siloles obtained from the CSD database.^[35] Geometrical parameters of **7d**, obtained from X-ray analysis are, in general, very well reproduced, including the bond and torsion angles. The well-known over-estimation of bond lengths by density functional methods, especially manifest in the carbon–heteroatom bonds, does not exceed 3.3% in any case.

The bond lengths and angles of the silole moiety and phenyl rings in the other diradicals are very similar to those of **7d**. Moreover, the geometrical parameters of the radical substituents are in the range of the data reported for other *tert*-butylnitroxide radicals. Therefore, this discussion will focus on the torsion angles between the aromatic spin-bearing units, the phenyl rings, and the central silole group, which are collected in Table 2. Coordinates of the minimum geometries for **7a** to **7d** are included in the Supporting Information (Tables S1 to S4). These torsion angles should determine the degree of delocalization/spin polarization of the

Table 2. Torsion angles [$^\circ$] in diradicals **7**.^[a]

	7a	7b	7c	7d (opt.)	7d (X-ray)
silole–Ph ^{A[B]}	41.1	41.3	72.9/71.0	53.2	47.2
silole–Ph ^B	58.7	59.1	53.8/54.0	55.7	60.4
(CH ₃ –Si–CH ₃)–silole	85.2	85.5	87.7	85.9	82.5
Ph ^{A/C} –(CNO)	3.1/2.9	6.4/6.5	74.3/76.5	14.3	17.0
Ph ^A –C ₃ N ₂	–	–	–	–	–
Ph ^A –Ph ^C	–	33.6	–	–	–

[a] Only one entry if both values are identical. [b] See Scheme 1 for the labeling of the aromatic rings.

unpaired electrons from the radical moieties onto the silole core of the molecule.

All compounds have a propeller-like arrangement of the four phenyl rings, as found in the crystal structure of **7d** (Figure 3a) and also reported for other tetraphenyl-substituted siloles,^[2,19] while the two methyl substituents on the silicon atom are nearly perpendicular to the mean plane of the SiC₄ ring. Therefore, the molecular geometries approach C₂ symmetry, even though the optimizations were performed without any constraints. The torsion angles of the nonsubstituted phenyl rings at the 3- and 4-positions of the central silole ring are larger than those of the radical-bearing phenyl rings in the 2- and 5-position owing to the larger steric interactions with two neighboring rings in the former as compared with just one for the latter ring. An exception is found for diradical **7c**, in which the larger size of the aromatic groups, caused by the additional fused rings D, enforces a torsion angle between the naphthyl and silole ring which is 20–30° larger than in the others, leading to an almost perpendicular arrangement of the two rings (Figure 3b). The same degree of steric hindrance is also seen between the naphthyl and nitroxide groups in **7c**, leading to large torsion angles of 74.3° and 76.5°, while in the cases of **7a** and **7b**, the phenyl ring and radical-bearing units are almost coplanar, and only a slight deviation from planarity is found in **7d** with torsion angles of 17.0° and 14.3° for the X-ray and optimized geometries, respectively. The torsion angle between both phenyl rings in the biphenyl unit of **7b** is 33.6°.^[35]

Geometry of the thiophene-bridged diradical 12: Crystals of **12** obtained by slow evaporation of a dichloromethane solution were subjected to X-ray diffraction analysis at 150 K. Compound **12** crystallizes in the orthorhombic crystal system in the *Pna*2₁ space group (Figure 4). The crystal lat-

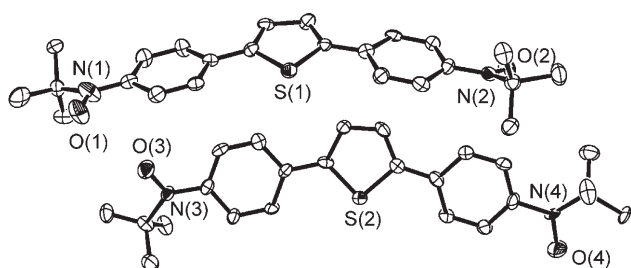


Figure 4. ORTEP view of **12** (50% probability).

tice structure consists of pairs of independent molecules *A* and *B* forming an herringbone pattern along the *b* axis (see Figure S1 in the Supporting Information). An examination of the molecular structure shows that the mean plane of the terminal phenyl rings is tilted relative to the central thiophene ring by 5.0° and 8.5° for molecule *A*, and 11.8° and 7.2° for molecule *B*, respectively. These values, as well as the bond lengths of the π system, are in the range of those reported for the related 2,5-diarylthiophenes crystal struc-

tures SUSNEZ^[36] and FEJRUH.^[37] The torsion angles between the nitroxide moiety and the phenyl ring are 20.9° and 3.2° for molecule *A* and 23.1° and 1.8° for molecule *B*, respectively. While the first torsion angle values are not uncommon in phenyl-substituted nitroxide radicals (see above), the second ones are unusual,^[38,39] and closer to the range of values reported for benzoquinonimine-*N*-oxide derivatives (3.3°).^[40,41] To check whether this structure reflects either a benzenoid or a quinonoid form in the crystal lattice, the 2,5-diphenylthienyl bond lengths for **12**, crystal structures SUSNEZ,^[36] FEJRUH (benzenoid forms),^[37] VIZBUB^[42] and QIPQAH (quinonoid forms)^[43] were compared (see Figure S2 and Table S5 in the Supporting Information). Interestingly, the bond lengths in the thiophene ring are not greatly affected by the structural modifications that accompany the transformation from a benzenoid form to a quinonoid form. More pronounced is the elongation of the C3–C4 and C4–C5 bonds in the adjacent phenyl rings that reaches $\approx 10\%$ and the concomitant shortening of the C2–C3 and C5–C6 bonds ($\approx 5\%$). Therefore, since the bond lengths found for compound **12** are closer to the range of values measured for benzenoid forms, we assume that the diradical probably adopts this structure in the crystal.

Electronic absorption spectra: The UV/Vis spectra of freshly prepared diradicals and their parent hydroxylamines were measured in chloroform. The resulting data are summarized in Table 3, which also contains the data on silole **1** for com-

Table 3. UV/Vis absorption spectral data for dihydroxylamines **6** and diradicals **7**.^[a]

Compound	1	6a	7a	6b	7b	6c	7c	6d	7d
$\pi-\pi^*_{\text{Ar-NO}}$ ^[b]	–	–	300	–	323	–	296	–	285
$\pi-\pi^*_{\text{silole}}$	359	366	420	391	400	351	363	360	362
$n-\pi^*_{\text{NO}}$	–	–	448	–	451	–	450	–	450

[a] 10^{−3} M solutions in CHCl₃. [b] Transition λ_{max} values given in nm.

parison. For all silole derivatives, the spectra are dominated by a broad absorption at $\lambda \approx 350\text{--}420$ nm that is characteristic of the $\pi-\pi^*$ transition originating from the silole ring.^[2] The diradicals are characterized by two additional absorption bands at $\lambda \approx 300$ nm and 450 nm attributed to the Ar–NO $\pi-\pi^*$ and N–O $n-\pi^*$ transitions, respectively. From an examination of the peak positions of the $\pi-\pi^*$ transitions (Table 3), it follows that these transitions are affected by three factors: 1) by the nature of the aryl groups in the 2,5-positions (phenyl versus naphthyl), 2) by the electron-withdrawing effects induced by the substituents, and 3) by the substituent position relative to the silole ring. Therefore, the conversion of the NOH groups to NO[•] leads to a bathochromic shift of the silole ring $\pi-\pi^*$ transition in every case. A minor red-shift of 2 nm is also observed for diradicals **7d** with the nitroxide groups in a *meta* orientation with respect to the silole ring. Although they are connected in a *para* orientation, which should promote larger electronic effects of

the substituents, **7b** and **7c** only show a moderate red-shift of 9 and 12 nm, respectively, compared to the 54 nm of diradical **7a**, which thus exhibits the largest shift in the series. Such differences might be ascribed to the different torsion angles as revealed by the molecular structures (Table 2). Thus, changing a biphenyl (**7b**) to a naphthyl (**7c**) ring does not seem to markedly affect the overall electronic effects induced by the oxidation of the hydroxyl groups because the combination of torsion angles and distances lowers π -conjugation. Diradical **12**, with a lower steric hindrance and larger conjugation, however, shows more drastic changes upon oxidation. The unique sharp absorption band observed at 344 nm for the bishydroxylamine, experiences a large red-shift to yield a very broad absorption at 391 nm, whereas three new absorption bands appear at 444, 479, and 551 nm. These modifications strongly suggest that diradical **12** undergoes an electronic reorganization in solution (vide infra). The structural stability of the silole diradicals was also checked by UV/Vis spectroscopy. With the exception of **7a**, the spectra of all the siloles remained identical for more than two weeks in solution and for several months in the solid state. In contrast, four new absorption bands at 309, 364, 401, and 570 nm appear in the spectrum of **7a** when the diradical remains in solution for one day. These new absorption bands are similar to those observed for **12**, indicating that both diradicals experience the same electronic reorganization. Actually, a similar behavior was observed for diradicals that correspond to an open-shell resonant form of a closed-shell structure.^[44] Basically, diradicals that are connected through the *para* position of a phenyl ring of a more extended π system quickly undergo an electronic rearrangement of their backbone leading to diamagnetic quinonoidal structures.^[30,40,41,45–48] From the spectroscopic point of view, quinonoidal structures are characterized by π - π^* transitions at about 320, 404 ($C=N^+-O^-$),^[41,49] and 550 nm (terphenylquinone).^[30] The data strongly suggests that diradicals **7a** and **12** undergo an electronic rearrangement to adopt quinonoidal structures, as previously found in related systems.

Electron paramagnetic resonance spectra: EPR spectra of the diradicals in degassed dichloromethane solutions were measured in the temperature range 4–298 K. At 298 K, the spectra of siloles **7a–d** and **12** (Figure 5 a) show a well-resolved symmetrical pattern consisting of five lines with intensities close to 1:2:3:2:1 attributed to hyperfine coupling between two equivalent nitrogen nuclei. The values found for the apparent hyperfine coupling constants with the N atom (Table 4) are, as expected, one half of the related constant found for monoradical derivatives (vide infra). Moreover, the spectra of such bisnitroxide diradicals indicate that, in each

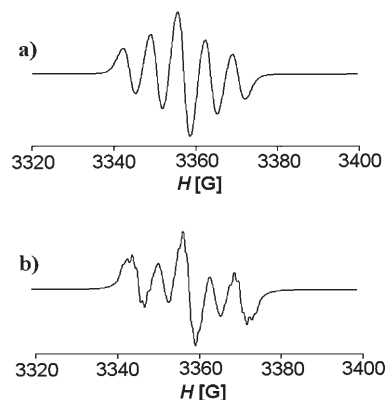
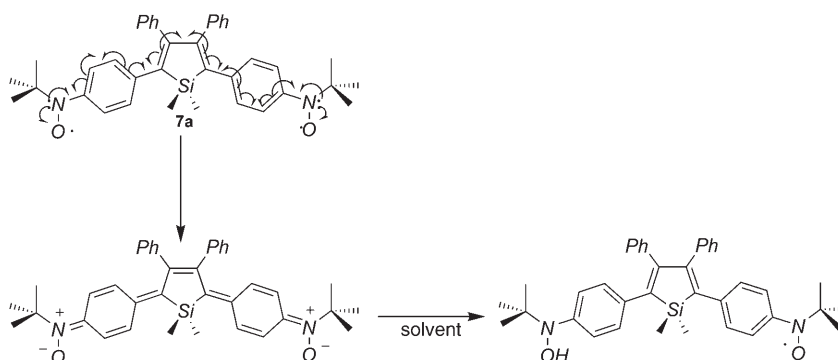


Figure 5. Room-temperature EPR spectra (in CH_2Cl_2) of diradical **7a**: a) freshly dissolved and b) after three days in solution.

Table 4. Apparent hyperfine coupling constants [Gauss] and diradical purities [%] obtained by simulation of EPR spectra of freshly prepared dilute solutions.

Diradical	7a	7b	7c	7d	12
a_N	5.65	5.81	6.84	6.59	5.97
diradical purity	90	95	97	97	89

case, the exchange coupling parameter J is substantially larger than the nitrogen hyperfine coupling constant ($|J| \gg a_N$). In accordance with the UV/Vis data (vide supra), the spectra of degassed solutions of diradicals **7b–d** remain unchanged for at least two weeks when stored in the dark, while the spectra of **7a** and **12** recorded after one day show several modifications indicative of a structural/electronic rearrangement in solution. Such modifications include an alteration of the relative peak intensities of the quintet and the appearance of a new hyperfine structure in the two outer lines and the central line that might be attributable to the concomitant presence of the diradical and a monoradical that have similar chemical structures. As previously described by Forrester et al.,^[46] the formation of monoradical species derived from bisnitroxides in solution might originate from the abstraction of a hydrogen atom from the solvent by the reactive bisnitrones that result from the quinonoidal rearrangement of the parent diradicals (Scheme 4). As a result, a monoradical hydroxylamine is generated,



Scheme 4. Quinonoidal rearrangement of diradical **7a**.

which gives rise to the additional structured signals that are observed in the EPR spectrum overlapped to the diradical signal. For **7a**, no further evolution is noticed in the EPR spectra after three days and the resulting pattern can be fully simulated as a mixture of 83% diradical of **7a** and 17% of a *para*-substituted phenyl-*tert*-butylnitroxide monoradical with the following hyperfine coupling constants: $a_N = 11.4$ G, $a_{\text{Hortho}} = 2.08$ G and $a_{\text{Hmeta}} = 0.85$ G (Figure 5b).^[50] Similar hyperfine coupling constants were found for diradical **12** after three days in solution. From the simulated spectra, a mixture of $\approx 25\%$ of monoradical and 75% of diradical was obtained. Interestingly, this composition remains almost constant until the disappearance of the EPR signal is observed after a period of three weeks in solution.

EPR spectra of freshly prepared diradicals **7a–d** and **12** in glassy matrices at 100 K gave broad signals that show a fine structure. These signals correspond to the intermolecular $\Delta M_S = 1$ transition of diradicals and originate from the weak dipolar coupling of the two unpaired electrons (Figure 6). The determination of zero-field splitting (ZFS)

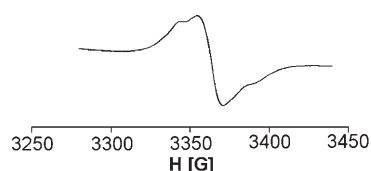


Figure 6. Typical EPR spectrum obtained in frozen dichloromethane at 4 K for diradicals **7a, c, d**, and **12**.

parameters from the simulation of the $\Delta M_S = 1$ signals^[51] could only be carried out for diradicals **7a, c, d**, and **12** (Table 5) because dipolar interactions in diradical **7b** are

Table 5. EPR parameters used for the simulation of the $\Delta M_S = +1$ signals of diradicals in frozen solution at 100 K.^[a]

Diradical	g_x	g_y	g_z	D [Gauss]	E [Gauss]
7a	2.005	2.005	2.005	30	0
7c	2.005	2.005	2.005	12.5	0
7d	2.008	2.005	2.002	16	0
12	2.005	2.005	2.005	31	0

[a] In dichloromethane glass.

weak compared to the hyperfine coupling constants. The average interspin distances were estimated to be 10 Å for diradicals **7a** and **12** and 13 Å for diradical **7c** using the point-dipole approximation.^[52] A comparison of the average interspin distances with the distance between the two NO groups obtained from the DFT-optimized geometries (NO...NO: 15.3 Å for **7a** and **12**, and 15.2 Å for **7c**) leads to the conclusion that the spin delocalization through the aromatic rings is much more effective in **7a** and **12** than in **7c** or **7d**. Moreover, the D parameter of **7c** is even smaller than that of **7d** in which the distance between the NO

groups is slightly smaller.^[19] This result is in agreement with the large torsion angles that are found for **7c** (Table 2) that disrupts π conjugation and decreases spin delocalization.

Decreasing the temperature below 80 K allows the observation of a signal at a field of ≈ 1715 G that is attributed to the $\Delta M_S = 2$ transition in the thermally populated triplet state of diradicals **7b–d**. This half-field signal is not observed for **7a** and **12**, even when large signal amplification and high concentrations are used. On further lowering of the temperature, a pronounced increase in the intensity of the $\Delta M_S = 1$ transition is noticed for diradicals **7b–d**, whereas a different behavior is observed for **7a** and **12**. For the latter compounds, the signal intensity decreases to a minimum at 35 K for **7a** and at 50 K for **12**, and then slightly increases down to the lowest temperatures attainable. It is worth noting that the increase of the $\Delta M_S = 1$ signal at very low temperatures is more pronounced with aged samples. Since the intensity of the $\Delta M_S = 1$ transition is proportional to the molar paramagnetic susceptibility of the sample, this behavior might originate from the simultaneous presence of either the diradical species, in which antiferromagnetic interactions take place between the unpaired electrons, and the monoradical species; as suggested by the isotropic room temperature spectrum (vide supra).

To determine the nature and the strength of magnetic coupling between the spin-bearing moieties in diradicals **7b–d**, the intensity of the $\Delta M_S = 2$ transition was measured as a function of the temperature between 4 and 30 K in frozen dichloromethane. In each case, as the temperature was decreased, the $\Delta M_S = 2$ signals, attributed to the triplet state, increased in intensity. A plot of the dependence of the intensity of this signal versus the reciprocal of the absolute temperature (Curie plot) is given in Figure 7 for diradical

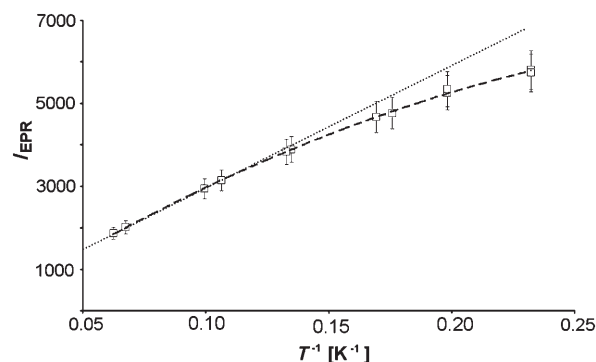


Figure 7. Temperature dependence of the EPR signal intensities of the $\Delta M_S = 2$ transition for diradical **7b** in frozen dichloromethane. The dashed curve shows the evolution of the signal using the spin-pair Bleaney–Bowers model (see text). The dotted line shows the variation of the signal expected for uncorrelated spins.

7b. The observed deviation of the intensity from the Curie Law strongly suggests that diradicals **7b–d** exist in a singlet ground state with an accessible thermally populated triplet state.

To evaluate the singlet–triplet energy gap, $\Delta E_{T-S}/k_B$, the Curie plots for diradicals **7b–d** were analyzed with the Bleaney–Bowers model [Eq. (1)], which describes the magnetic behavior of isolated diradicals.^[53] The best fit of the experimental data to Equation (1), where C is a constant to fit the sample intensity, and ΔE_{T-S} is the singlet–triplet energy gap, indicates that the energy separation between the accessible thermally populated triplet state and the singlet ground state are 3.5, 2.1, and 5.6 cm^{-1} for diradicals **7b**, **7c**, and **7d**, respectively.

$$I_{\text{ESR}} = \frac{C}{T} \left[\frac{1}{3 + \exp\left(\frac{\Delta E_{T-S}}{k_B T}\right)} \right] \quad (1)$$

Magnetic susceptibility measurements:^[54] The magnetic properties of diradicals **7a–d** and **12** were also investigated on polycrystalline samples in the temperature range of 2 to 300 K. The temperature dependence of the molar magnetic susceptibility, χ_M , for compounds **7a**, **7c**, and **12** is given in Figure 8 in the form of a plot of $\chi_M T$ versus T since they are representative of the two types of magnetic behavior that are observed for this series of diradicals. For diradicals **7b–d**, the $\chi_M T$ value of $\approx 0.63 \text{ cm}^3 \text{ K mol}^{-1}$ remains constant from 300 K down to ≈ 20 K and a slight decrease at lower temperatures is observed. Such behavior is indicative of very weak antiferromagnetic interactions between the spin carriers. In contrast, $\chi_M T$ values of 0.33 $\text{cm}^3 \text{ K mol}^{-1}$ and 0.28 $\text{cm}^3 \text{ K mol}^{-1}$ were found at 300 K for compounds **7a** and **12**, respectively. Such values are well below the expected contribution of two noncorrelated $S = 1/2$ spins (0.75 $\text{cm}^3 \text{ K mol}^{-1}$). Moreover, the $\chi_M T$ values rapidly decrease as the temperature is lowered, finally reaching a plateau value of 0.06 $\text{cm}^3 \text{ K mol}^{-1}$ below 28 K for **7a** and 0.10 $\text{cm}^3 \text{ K mol}^{-1}$ below 55 K for **12**. For these two compounds, rather strong antiferromagnetic interactions are operative between the two radical units. In the lower temperature domain, the observation of non-zero $\chi_M T$ values is ascribed to the presence of a minor fraction of monoradical species in the samples that result from the structural/electronic rearrangement and hydrogen abstraction of **7a** and **12**, as shown by the EPR and the UV/Vis studies described above.

The magnetic behavior of compounds **7b–d** has been analyzed by a modified dimer model with the spin Hamiltonian.^[53,55] The corresponding expression for $\chi_M T$ is given by Equation (2):

$$\chi_M T = f \left[\frac{2 N g^2 \beta^2}{k_B} \frac{1}{3 + \exp(-2J/k_B T)} \right] \quad (2)$$

where J represents the exchange parameter, g is the isotropic Landé constant, β is the Bohr magneton, and k_B is the Boltzmann constant. A purity factor, f , was introduced to account for the possible presence of diamagnetic fractions caused by the instability of these diradicals.^[56] The best fit to

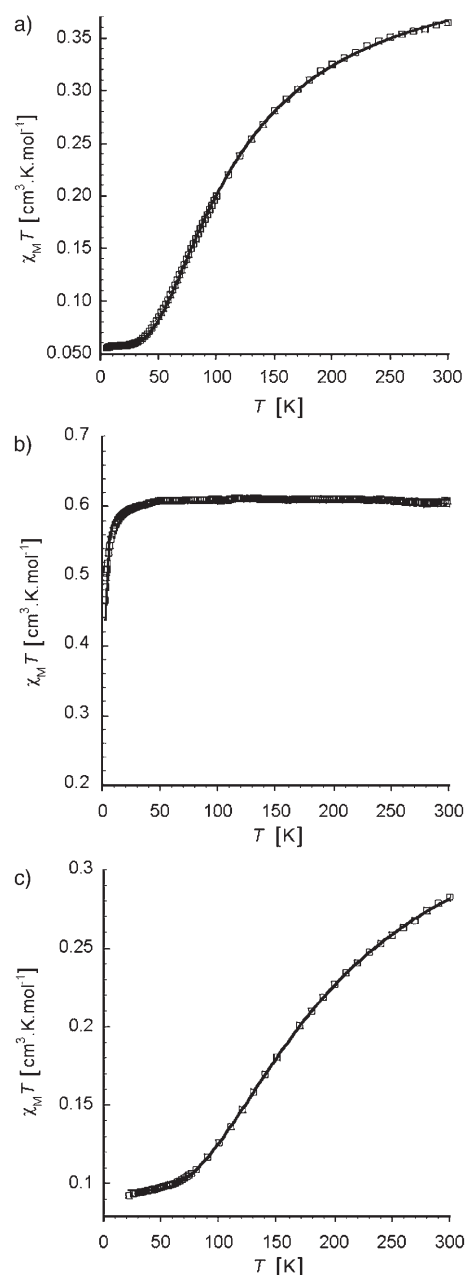


Figure 8. Temperature dependence of the experimental (\square) and calculated (—) $\chi_M T$ behavior for a) **7a**, b) **7c**, and c) **12**.

the experimental data yielded $J = -1.8 \text{ cm}^{-1}$ with $f = 0.84$ for **7b**, $J = -1.3 \text{ cm}^{-1}$ with $f = 0.81$ for **7c**, and $J = -4.2 \text{ cm}^{-1}$ and $f = 0.96$ for **7d**. The introduction of a Weiss constant, θ , in the analytical expression did not significantly modify the resulting parameters. These exchange parameters are very similar to the singlet–triplet gaps ($\Delta E_{T-S} = -2J$) obtained from the glassy matrix EPR studies and, therefore, they can be attributed to an intramolecular interaction taking place between the two radical units. The magnetic behavior for compounds **7a** and **12** has also been analyzed by a dimer model, but including a paramagnetic contribution

arising from monoradical $S = 1/2$ species. The rather low values observed for $\chi_M T$ at 300 K suggest the presence of a nonmagnetic fraction and, therefore, the ratios of di- and monoradicals have been taken as relative to the whole sample. The expression used to analyze the experimental data is given by Equation (3):

$$\chi_M T = a \left[\frac{2Ng^2\beta^2}{k_B[3 + \exp(-2J/k_B T)]} \right] + b \left[\frac{Ng^2\beta^2}{2k_B} \right] \quad (3)$$

where a and b refer to the molar fraction of di- and monoradical species, respectively. The best fit of the experimental data, taking $g = 2$, for **7a** yielded an exchange parameter $J = -142 \pm 0.3 \text{ cm}^{-1}$ with a sample composition in magnetic species of 51% of diradical and 15% of monoradical. For compound **12**, the resulting parameter was: $J = -248 \pm 1 \text{ cm}^{-1}$ with a sample composition of 39% of diradical and 25% of monoradical.

Theoretical calculation of spin densities and exchange parameters: The atomic spin densities calculated in single-point runs at the UB3LYP/6-31+G* level are collected in Table 6 for *tert*-butylnitroxides **7a–d**. Spin densities on the *tert*-butyl group are not included because they are very small and comparable to values observed both experimentally or deduced by calculation for other radicals of the same kind.^[38,57–59]

Table 6. Mullikan atomic spin densities for **7a–d** calculated at the UB3LYP/6-31+G* level.

Atom ^[a]	7a Optimized geometry	7b Optimized geometry	7c Optimized geometry	7d ^[b] X-ray structure	7d ^[b] Optimized geometry
N	0.3757/0.3747	0.3719/0.3785	0.4304/0.4326	0.4017	0.4020
O	0.4714/0.4728	0.4809/0.4765	0.5206/0.5235	0.4764	0.4789
C4 in Ph ^C		-0.1200/-0.1185			
C3/C5 in Ph ^C		0.1352/0.1320			
		0.1264/0.1285			
C2/C6 in Ph ^C		-0.0631/-0.0687			
		-0.0712/-0.0671			
C1 in Ph ^C		0.1175/0.1177			
C4 in Ph ^A	-0.1306/-0.1293	-0.0240/-0.0226	-0.0233/-0.0320	0.1461	0.1634
C3/C5 in Ph ^A	0.1257/0.1261	0.0226/0.0220	0.0349/0.0307	-0.0588	-0.0652
	0.1306/0.1325	0.0222/0.0220	0.0165/0.0307	-0.1351	-0.1487
C2/C6 in Ph ^A	-0.0679/-0.0687	-0.0127/-0.0138	-0.0111/-0.0085	0.1196	0.1238
	-0.0653/-0.0650	-0.0123/-0.0121	-0.0070/-0.0063	0.1270	0.1346
C1 in Ph ^A	0.1228/0.1181	0.0232/0.0219	0.0204/0.0152	-0.0607	-0.0696
C7 in Ph ^D			0.0073/0.0059		
C8 in Ph ^D			-0.0053/-0.0041		
C9 in Ph ^D			0.0073/0.0057		
C10 in Ph ^D			-0.0026/-0.0021		
Si	0.0054	0.0012	0.0017	-0.0051	-0.0061
Si-CH ₃	-0.0013/-0.0001	-0.0001/0.0000	-0.0001/0.0000	0.0008	0.0005
Silole-C2/C5	0.0277/-0.0062	-0.0025/-0.0003	-0.0001/0.0146	0.0069	0.0093
Silole-C3/C4	0.0125/0.0395	0.0045/0.0062	0.0084/-0.0218	-0.0085	-0.0081
C1 in Ph ^B	-0.0060/-0.0062	-0.0009/0.0016	0.0001/0.0008	0.0003	-0.0010
C2/C6 in Ph ^B	0.0044/0.0042	0.0008/0.0007	0.0000/0.0000	-0.0001	0.0002
	0.0039/0.0038	0.0007/0.0007	-0.0002/0.0001	-0.0043	-0.0059
C3/C5 in Ph ^B	-0.0019/-0.0018	-0.0004/-0.0003	0.0001/0.0000	-0.0006/	0.0035/
	-0.0013/-0.0012	-0.0002/-0.0001	0.0002/0.0000	0.0028	-0.0002
C4 in Ph ^B	0.0032/0.0033	0.0007/0.0006	-0.0001/0.0001	0.0004	-0.0002

[a] See Scheme 1 for the labeling scheme. [b] Only one value is reported because the two halves of the molecule are identical on account of its C_2 symmetry.

The spin density on the spin-bearing units is as expected, with a large positive spin density on the NO groups. The spin density then spreads out onto the adjacent phenyl ring *A* (see Scheme 1) on account of the direct delocalization of the unpaired electron onto the phenyl ring in the latter, and follows the sign alternation principle.^[57,58] The only exception is found for naphthyl-substituted **7c**, in which the large NO–naphthyl torsion angles of 74.3° and 76.5° prevent delocalization of the unpaired electron from the NO group, therefore leading to spin densities on the *A* ring of the naphthyl group that are one order of magnitude smaller than in the other *tert*-butylnitroxides **7a**, **7b**, and **7d**, while the fused ring *D* carries an even smaller spin density. Furthermore, in the biphenyl-substituted compound **7b**, only ring *C*, directly connected to the NO group, carries a spin density comparable to **7a** and **7d**, while on ring *A*, the spin density is smaller by a factor of \approx five owing to the Ph–Ph torsion angle of 33.6°, which prevents further delocalization of the unpaired electron from ring *C* to ring *A*. This diradical is another example of conformational effects modulating the spin density distribution in this series of compounds.

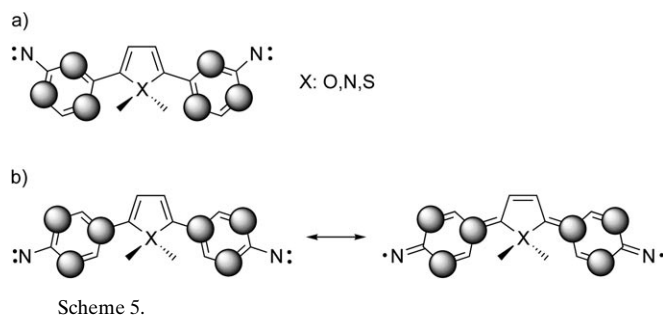
The spin density on the silicon atom is small (< 0.01) in all cases and the sign systematically depends on the position (*meta* versus *para*) where the spin-bearing moiety is attached to the aromatic ring. It also correlates with the amount of spin density on the phenyl ring *A* attached to the central silole ring. In cases with little spin density on ring *A*, either because it only originates from spin polarization or owing to conformational constraints that prevent efficient delocalization of the unpaired electron (**7b** and **7c**), the spin density on the silicon atom is very small (< 0.002). In contrast, in radicals **7a** and **7d**, which have larger spin densities on phenyl ring *A*, the spin density on the Si atom is larger by a factor of three to five (**7a**: 0.0054, **7d**: -0.0051 (X-ray), -0.0061 (optimized)). The spin density on the methyl substituents on the silicon atom and the 3- and 4-phenyl rings *B* is very small and approaches zero in all compounds. Interestingly, no clear correlation between the sign and magnitude of the spin density and conformational preference can be drawn for the carbon atoms of the silole ring, especially in those cases with no imposed symmetry (**7a–d**). In general, there is little unpaired spin on the carbon atoms (< 0.01 in almost all cases); however, the

magnitude and sign are in some cases different for the C2/C5 and C3/C4 atoms, even though all molecules possess near- C_2 symmetry. This might be caused by subtle differences in the conformations of the two halves of the molecules or by a slight contamination of the triplet states by close-lying higher spin states, as is apparent in the deviation of \hat{S}^2 from the expected value of 2.0 (**7a**: 2.0292, **7b**: 2.0284, **7c**: 2.0100, **7d**: 2.0211 (X-ray), 2.0215 (optimized)).

To test if the computational methods used are able to correctly reproduce both the sign and magnitude of the exchange parameter J determined experimentally for **7d**, the energies of the broken-symmetry singlet and high-spin triplet states of **7d** were determined at the X-ray structure coordinates and optimized geometry with high accuracy (UB3LYP, 6-31+G* basis set, tight convergence, ultrafine grid). The values calculated for J of -0.55 cm^{-1} (X-ray) and -0.39 cm^{-1} (optimized) from the S-T gap without spin projection using a Hamiltonian of $\hat{H} = -2J\hat{S}_1\hat{S}_2$ are somewhat smaller than the experimental values ($J = -4.2 \text{ cm}^{-1}$, SQUID, microcrystalline powdered sample and -5.6 cm^{-1} , EPR, frozen solution); however, they do confirm the weak antiferromagnetic coupling mediated by the silole ring in **7d**.

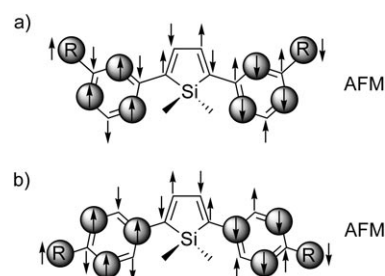
Magnetic coupling mechanism in silole-bridged diradicals:

There are two main issues associated with the experimental results described here: first, how do nitroxide radicals interact magnetically when linked by a silole ring? Second, what is the role of the silicon atom in mediating the magnetic interaction when incorporated in the silole ring? With respect to the first issue, some work has recently been dedicated to the study of systems with paramagnetic centers connected through the 2,5-positions of heteropentacycles such as furans, pyrroles and thiophenes, since these systems with non-alternant conjugation may lead the way to a large number of intramolecular magnetic exchange possibilities.^[48,60-62] Among them, the thiophene ring has been shown to act more efficiently than the benzene ring itself since it is more electron-rich and it is sterically less demanding than the latter.^[61] The influence of the spin-bearing sites connected to five-membered rings has also been extensively studied. For instance, the connection of two *meta*-phenylnitrene units leads to systems termed as pseudo-disjoint because spin-bearing units are connected to the central ring through sites bearing minimal spin density (Scheme 5a). These sys-



tems usually display singlet ground states with low-lying excited multiplet states. On the other hand, the attachment of two *para*-phenylnitrene units provide a connection through spin-bearing sites that leads to localized quinonoidal diradical systems because they actually correspond to an open-shell form of a Kekulé π -conjugated molecule (Scheme 5b).

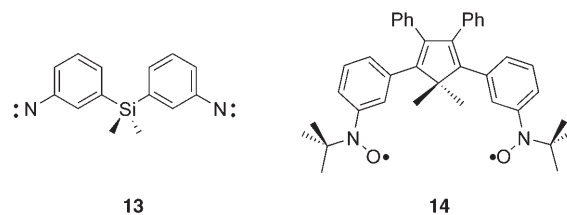
With respect to this classification, we will divide the molecules described herein into two main categories. Diradical **7d** will be classified in the pseudo-disjoint category and the others will be classified into the non-pseudo-disjoint one. Obviously, in all cases, antiferromagnetic interactions between the paramagnetic centers are expected both from a valence-bond and spin-polarization point of view (Scheme 6). However, a careful examination of their mag-



Scheme 6. Expected magnetic interaction in silole-bridged diradicals on the basis of the spin-polarization mechanism. Grey circles depict regions with positive spin density.

netic properties will be useful to address the second question concerning the role of silicon in the mediation of magnetic interactions in the silole coupler.

As mentioned above, the pseudo-disjoint category only includes diradical **7d**, which displays weak intramolecular antiferromagnetic interactions in the solid state as well in a frozen solution.^[19] At first glance, the nearly planar conformation around the silicon atom in the silole linker accounts for the different behavior with respect to the flexible dinitrene **13** (Scheme 7) for which no magnetic interaction was



Scheme 7.

observed.^[63] Though the spin density on the silicon atom is quite low in all cases (Table 6), this observation suggests that it might be involved in the exchange interaction pathway. Since the exchange interaction can either be mediated by the π system of the silole ring or by a σ pathway involving the silicon atom, the calculations were repeated for the

singlet and triplet states of model compound **14** in which the silicon atom was replaced by a sp^3 -hybridized carbon atom, while otherwise retaining the X-ray structure without geometry relaxation. A value of $J = -0.54 \text{ cm}^{-1}$ was obtained, which is almost identical to the one calculated for the parent compound. Though the energy differences are very small, we feel that they can accurately be reproduced within a series of compounds and give some evidence that the exchange interaction is mainly mediated by the π system of the silole ring.^[57,64,65]

With regard to the second category (non-pseudo-disjoint), two classes of molecules, named here as Class A and Class B, can be distinguished both from magnetic measurements and bonding considerations.

Class A diradicals: The first class of compounds includes diradicals **7a** and **12** that correspond to the open-shell resonant form of a classical Kekulé π -conjugated molecules.^[66] In such systems, the spin coupling is often sufficient to induce pairing of the single electrons leading to closed-shell structures. This is indeed the case with **7a** and **12**, which exhibit rather strong antiferromagnetic interactions and experience a structural/electronic rearrangement to the corresponding quinonoidal structure. The experimental exchange parameter for these diradicals is very large ($J = -142 \text{ cm}^{-1}$ for **7a** and $J = -248 \text{ cm}^{-1}$ for **12**), thus underlining a strong dependence of the exchange interactions on the nature of the central heterocycle. At least three factors may be invoked to explain such a difference: conformation, spin density, and heteroatom effect. Conformational and spin density effects are already known to play an important role in the magnetic exchange modulation for TMM-type diradicals.^[64,67] It has been shown that the exchange coupling parameter can be closely correlated to the average side-ring torsion angles (φ_{av}) via a “Karplus–Conroy-type” equation [Eq. (4)], where the A term is related to the coupler and the spin density on the spin-containing group and the B term corresponds to the through-space antiferromagnetic interaction.

$$J = A \cos^2[\varphi_{av}] + B \quad (4)$$

If we assume that the through-space antiferromagnetic interaction is negligible (vide supra), and that the spin density carried by the side groups is similar for both compounds (see magnetic measurements above), then the $A(\mathbf{7a}):A(\mathbf{12})$ ratio should give an estimate of the ability of the central heterocycle to mediate antiferromagnetic interactions [Eq. (5)].

$$\frac{A(\mathbf{7a})}{A(\mathbf{12})} = \frac{J(\mathbf{12})\cos^2[\varphi_{av}(\mathbf{7a})]}{J(\mathbf{7a})\cos^2[\varphi_{av}(\mathbf{12})]} \quad (5)$$

For average torsion angles of 41.1° for **7a** and 12.3° for **12**, we find a value of 0.96 for the $A(\mathbf{7a}):A(\mathbf{12})$ ratio, whereas the $J(\mathbf{7a}):J(\mathbf{12})$ ratio is 0.57. This result indicates that both

the silole ring and the thiophene ring intrinsically act as antiferromagnetic couplers with the same efficiency. The presence of the additional phenyl rings at the 3,4-positions of the silole ring for **7a** induces torsion angles for the spin-bearing units that are responsible for the low value of the exchange parameter compared to **12**. On the other hand, the increased stability of **12** probably originates from the aromatic character of the thiophene compared to the silole unit. Indeed, as shown for phenyl-conjugated Kekulé-type dinitrenes,^[65] the tendency to maintain the aromaticity tends to favor the diradical structure over the quinonoidal one.

Class B diradicals: The second class of compounds, which includes diradicals **7b** and **7c**, also corresponds to the open-shell resonant form of Kekulé π -conjugated molecules. The main difference between these siloles and **7a** is that they have been designed to disfavor a quinonoidal rearrangement, either by inserting or by fusing an additional phenyl ring to the structure. The magnetic studies revealed weak antiferromagnetic interactions for this class of diradicals with an exchange parameter of $J = -1.8 \text{ cm}^{-1}$ and $J = -1.3 \text{ cm}^{-1}$ for **7b** and **7c**, respectively. This can be attributed to both the large separation (**7b**) and the large torsion angles (**7c**) between the spin bearing units. It is therefore not surprising to find very small values of spin density on the silicon atom by DFT calculations [Eq. (6)].

$$J = A \cos^2[\phi_{av}]\cos^2[\phi'_{av}] + B \quad (6)$$

Since the distance between the radical centers is very similar in diradicals **7a** and **7c**, we have checked if the exchange modulation observed for these diradicals is governed by conformational considerations. Modification of Equation (4) to take account of the average torsion angle between the phenyl ring and the *t*BuNO group (ϕ'_{av}) [Eq. (6)] allows the $A(\mathbf{7a}):A(\mathbf{7c})$ ratio to be determined. Using the torsion angles from Table 2, and setting B to zero we find that the $A(\mathbf{7a}):A(\mathbf{7c})$ ratio, which reflects the magnetic coupling ability of the silole, is equal to 1.05 whereas the $J(\mathbf{7a}):J(\mathbf{7c})$ ratio is equal to 94.7. For this class of diradical, too, the exchange mechanism appears to mainly involve the π system of the silole ring.

Conclusion

To study the ability of the silole ring to act as a magnetic coupler and to determine the role of the silicon atom in the magnetic exchange in such molecules, we have synthesized and investigated the magnetic properties of a series of diradicals in which the two spin-bearing units are linked by a non-alternant silole ring. The thiophene-coupled diradical **12** was also synthesized to provide a comparison with this well-known heteropentacycle. While compounds **7b**, **7c**, and **7d** are quite stable in solution and in the solid state, **7a** and **12** undergo partial electronic rearrangement to both a dia-

magnetic quinonoidal form and a monoradical species on account of the fact that they correspond to the open-shell form of a π -conjugated Kekulé structure. Geometry optimizations of silole-bridged diradicals at the UB3LYP/6-31G level accurately reproduce the experimental geometry available for comparison. Spin densities calculated with the larger 6-31+G* basis set and the same functional compare quite well with other reported calculations. Such spin densities along with the structural data obtained from the geometry optimizations, show how different mechanisms give rise to the spin density distribution (direct delocalization versus spin polarization) combined with conformational constraints determine the spin density at the core of the molecules. Thus, the connection across the 2,5-positions of spin-bearing units leads to intramolecular antiferromagnetic interactions that are modulated by the conformation of the molecules leading to singlet ground states. The weak antiferromagnetic exchange interaction between the two radical moieties, which is found experimentally in compound **7d**, could also be confirmed by theoretical calculations. An exchange parameter unaltered by substitution of silicon by carbon in a model compound suggests that the interaction mainly proceeds via the π -system of the silole ring. Finally, analyses of the data with a "Karplus–Conroy"-type equation allowed us to establish that the silole ring, as a whole, leads to a stronger exchange interaction between the two nitroxide radicals attached to its 2,5-positions than the thiophene ring. This increased efficiency probably originates from the non-aromaticity of the silole thus improving the magnetic interaction through it.

Experimental Section

Materials and methods: All reactions were routinely carried out under argon using standard Schlenck techniques. Solvents were distilled prior to use. THF was dried over sodium/benzophenone and distilled under argon. All commercial reagents were used as received. Bis(phenylethynyl)dimethylsilane^[68] was obtained by the reaction of dimethyldichlorosilane and phenylethynyllithium, which was prepared from *n*BuLi and phenylacetylene in ether. ¹H, ¹³C, and ²⁹Si NMR spectra were recorded on a Bruker Advance 200DPX spectrometer, the FT-IR spectra on a Thermo Nicolet Avatar320 spectrometer, the UV/Vis spectra on a Secomam Anthelie instrument, and the MS spectra on a Jeol JMS-DX300 spectrometer in a *m*-nitrobenzyl alcohol matrix. Elemental analyses were performed at the Service Central de Microanalyse of the CNRS, Vernaison (France). The ESR spectra were recorded on X-band Bruker Elexsys spectrometer. Magnetic measurements down to 2 K were carried out in a Quantum Design MPMS-5S SQUID susceptometer. All magnetic investigations were performed on polycrystalline samples. The molar susceptibility was corrected for the sample holder and for the diamagnetic contribution of all atoms by means of Pascal's tables.^[55,69]

1-[*N*-tert-butyl-*N*-(trimethylsilyloxy)amino]-4-bromobenzene (5a): An excess of triethylamine (21 mL, 150 mmol) was added to a solution of 1-[*N*-tert-butyl-*N*-(hydroxylamino)-4-bromobenzene (**4a**)^[29] 12.2 g, 50 mmol) in THF (100 mL). Chlorotrimethylsilane (19 mL, 150 mmol) in THF (50 mL) was added to the reaction mixture. After the mixture had been stirred at 45 °C for 20 h, the solvents were evaporated to yield a residue that was treated with pentane (200 mL) and then filtered. The filtrate was evaporated in vacuum to yield **5a** as an orange oil (14.1 g, 89%). ¹H NMR (CDCl₃, 298 K): δ = 0.01 (s, 9H), 1.10 (s, 9H), 7.16 (d,

$J(\text{H,H}) = 8 \text{ Hz}$, 2H), 7.37 ppm (d, $J(\text{H,H}) = 8 \text{ Hz}$, 2H); ¹³C{¹H} NMR (CDCl₃, 298 K): δ = 0.20, 26.48, 61.06, 118.11, 127.11, 130.76, 150.68 ppm; ²⁹Si NMR (CDCl₃, 298 K): δ = 22.23 ppm; IR (CHCl₃): $\tilde{\nu}$ = 1360 cm⁻¹ (N–O); MS (FAB+): m/z : 316 [M+H]⁺.

1-[*N*-tert-butyl-*N*-(trimethylsilyloxy)amino]-4-bromobiphenyl (5b): This compound was prepared starting from 1-[*N*-tert-butyl-*N*-(hydroxylamino)-4-bromobiphenyl **4b**]^[28] in a manner similar to the synthesis of compound **5a** (90%). ¹H NMR (CDCl₃, 298 K): δ = 0.03 (s, 9H), 1.16 (s, 9H), 7.30 (d, $J(\text{H,H}) = 8 \text{ Hz}$, 2H), 7.56–7.60 ppm (m, 6H); ¹³C{¹H} NMR (CDCl₃, 298 K): δ = 0.25, 26.63, 61.25, 121.44, 125.86, 128.84, 132.17, 136.46, 140.32, 151.29 ppm; ²⁹Si NMR (CDCl₃, 298 K): δ = 21.85 ppm; IR (CHCl₃): $\tilde{\nu}$ = 1361 cm⁻¹ (N–O); MS (FAB+): m/z : 392 [M+H]⁺.

1-[*N*-tert-butyl-*N*-(trimethylsilyloxy)amino]-4-bromonaphthalene (5c): This compound was prepared starting from 1-[*N*-tert-butyl-*N*-(hydroxylamino)-4-bromonaphthalene **4c** in a manner similar to the synthesis of compound **5a** (95%). ¹H NMR (CDCl₃, 298 K): δ = 0.04 (s, 9H), 1.10 (s, 9H), 5.46 (s, 1H), 7.79 (d, $J(\text{H,H}) = 8 \text{ Hz}$, 1H), 8.18 (d, $J(\text{H,H}) = 8 \text{ Hz}$, 1H), 8.53–8.56 ppm (m, 1H); ²⁹Si NMR (CDCl₃, 298 K): δ = 21.94 ppm; IR (CHCl₃): $\tilde{\nu}$ = 1361 (N–O); MS (FAB+): m/z : 366 [M+H]⁺.

1-[*N*-tert-butyl-*N*-(trimethylsilyloxy)amino]-3-bromobenzene (5d): This compound was prepared starting from 1-[*N*-tert-butyl-*N*-(hydroxylamino)-3-bromobenzene **4d** in a manner similar to the synthesis of compound **5a** (89%). ¹H NMR (CDCl₃, 298 K): δ = 0.02 (s, 9H), 1.13 (s, 9H), 7.49–7.12 ppm (m, 4H); ¹³C{¹H} NMR (CDCl₃, 298 K): δ = 0.19, 26.54, 61.31, 121.47, 124.17, 128.07, 127.93, 128.95, 153.18 ppm; ²⁹Si NMR (CDCl₃, 293 K): δ = 22.51 ppm; IR (CHCl₃): $\tilde{\nu}$ = 1361 (N–O); MS (FAB+): m/z : 316 [M+H]⁺.

Silole 6a: A mixture of lithium (0.2 g, 29 mmol) and naphthalene (3.71 g, 29 mmol) in THF (30 mL) was stirred at room temperature under argon for 5 h to form a deep green solution of lithium naphthalenide. To the mixture was added bis(phenylethynyl)dimethylsilane (**2**, 2 g, 7.7 mmol) in THF (20 mL). After stirring for 10 min, the reaction mixture was cooled to 0 °C and [ZnCl₂(tmen)] (tmen = *N,N,N',N'*-tetramethylethylenediamine) (7.82 g, 29 mmol) was added as a solid to form organozinc derivative **3**. After stirring for an hour at room temperature, a solution of **5a** (4.82 g, 15.3 mmol) in THF (20 mL) and [PdCl₂(PPh₃)₂] (0.28 g, 0.4 mmol) were added successively. The mixture was heated under reflux and stirred for 24 h. After hydrolysis with HCl (1M), the mixture was extracted with Et₂O. The combined organic layers were washed with brine, dried over MgSO₄, and concentrated. The resulting residue was subjected to column chromatography (neutral aluminum oxide, pentane/dichloromethane 80:20) to give 2.68 g (4.57 mmol) of **6a** (56%). M.p. 198 °C (decomp); ¹H NMR ([D₆]DMSO, 298 K): δ = 0.51 (s, 6H), 1.13 (s, 18H), 5.37 (s, 2H), 6.81–6.87 (m, 8H), 7.00–7.05 ppm (m, 10H); ¹³C{¹H} NMR ([D₆]DMSO, 298 K): δ = -2.67, 26.83, 60.18, 124.60, 127.14, 128.33, 128.41, 130.22, 135.48, 139.84, 141.02, 149.29, 153.81 ppm; ²⁹Si NMR ([D₆]DMSO, 298 K): δ = 7.46 ppm; IR (CCl₄): $\tilde{\nu}$ = 3589 (O–H), 1359 cm⁻¹ (N–O); UV/Vis (CCl₄): λ_{max} (log ϵ): 366 nm (1347, $\pi \rightarrow \pi^*$ silole); HRMS (FAB+): m/z : calcd for C₃₈H₄₅N₂O₂Si [M+H]⁺: 589.3250; found 589.3198; anal. calcd for C₃₈H₄₄N₂O₂Si: C 77.51, H 7.53; N 4.76, Si 4.77; found: C 77.55, H 7.59; N 4.82, Si 4.51.

Silole 6b: This compound was prepared starting from compound **5b** in a manner similar to the synthesis of compound **6a** (78%). M.p. 172 °C (decomp); ¹H NMR ([D₆]DMSO, 298 K): δ = 0.53 (s, 6H), 1.16 (s, 18H), 6.88–6.98 (m, 4H), 6.99–7.08 (m, 8H), 7.20–7.42 (m, 10H), 7.52–7.58 ppm (m, 6H); ¹³C{¹H} NMR ([D₆]DMSO, 298 K): δ = -2.86, 26.43, 61.15, 125.25, 125.26, 126.30, 126.82, 127.37, 128.56, 129.90, 130.24, 132.27, 132.37, 132.61, 137.54, 138.88, 139.47, 141.51, 154.69 ppm; ²⁹Si NMR ([D₆]DMSO, 298 K): δ = 8.18 ppm; IR (CCl₄): $\tilde{\nu}$ = 3590 (O–H), 1359 cm⁻¹ (N–O); UV/Vis (CCl₄): λ_{max} (log ϵ) = 391 nm (2.106, $\pi \rightarrow \pi^*$ silole); HRMS (FAB+): m/z : calcd for C₅₀H₅₅N₂O₂Si [M+H]⁺: 741.3877; found 741.3875; elemental analysis (%) calcd for C₅₀H₅₂N₂O₂Si: C 81.04, H 7.07, N 3.78, Si 3.79. found: C 80.95, H 7.09, N 3.85, Si 3.67.

Silole 6d: This compound was prepared starting from compound **5d** in a manner similar to the synthesis of compound **6a** (63%). M.p. 130 °C (decomp); ¹H NMR ([D₆]DMSO, 298 K): δ = 0.48 (s, 6H), 0.97 (s, 18H), 5.20 (s, 2H), 6.76–6.83 (m, 8H), 7.00–7.14 ppm (m, 10H); ¹³C{¹H} NMR

([D₆]DMSO, 298 K): $\delta = -3.21, 26.72, 59.92, 80.03, 122.57, 124.94, 125.49, 127.06, 127.315, 127.93, 128.35, 129.07, 130.18, 135.38, 139.04, 139.39, 141.99, 151.29, 154.30$ ppm; ²⁹Si NMR ([D₆]DMSO, 298 K): $\delta = 7.82$ ppm; IR (CCl₄): $\tilde{\nu} = 3589.7$ (O–H), 1363.2 cm⁻¹ (N–O); UV/Vis (CHCl₃): λ_{\max} (log ϵ) = 360 nm (4.83, $\pi \rightarrow \pi^*$ silole); HRMS (FAB+): m/z : calcd for C₃₈H₄₅N₂O₂Si [M+H]⁺: 589.3250; found 589.3243; elemental analysis calcd (%) for C₃₈H₄₄N₂O₂Si: C 77.51, H 7.53, N 4.76, Si 4.77; found: C 77.47, H 7.58, N 4.74, Si 4.56.

Silole 6': This compound was prepared by a Pd⁰-catalyzed crosscoupling reaction between 1,4-dibromonaphthalene (6 equiv) and organozinc derivative **3** in a manner similar to the synthesis of compound **6a** (40%). M.p. 228–230 °C; ¹H NMR ([D₆]DMSO, 298 K): $\delta = 0.30$ (s, 6H), 6.78–6.94 (m, 10H), 7.54–7.68 (m, 8H), 8.08–8.12 (m, 2H), 8.23–8.28 ppm (m, 2H); ¹³C{¹H} NMR ([D₆]DMSO, 298 K): $\delta = -3.66, 126.05, 126.59, 126.83, 127.40, 127.49, 127.52, 127.84, 129.62, 130.11, 130.50, 132.35, 134.31, 138.42, 139.58, 143.41, 155.90$ ppm; ²⁹Si NMR ([D₆]DMSO, 298 K): $\delta = 11.63$ ppm; UV/Vis (CHCl₃): λ_{\max} (log ϵ) = 351 nm (4.975, $\pi \rightarrow \pi^*$ silole); HRMS (FAB+): m/z : calcd for C₃₈H₂₈Br₂Si [M]⁺: 670.0327; found 670.0349; elemental analysis calcd (%) for C₃₈H₂₈Br₂Si: C 67.87, H 4.20, Si 4.18; found: C 67.98, H 4.09, Si 4.03.

Silole diradical 7a: To a solution of **6a** (0.77 g, 1.31 mmol) in CH₂Cl₂ (40 mL) was added freshly prepared Ag₂O (0.64 g, 2.73 mmol). The mixture was stirred for 45 min at 0 °C and filtered. The solvent was removed under vacuum and the resulting deep red solid was purified by column chromatography (neutral aluminum oxide, pentane/dichloromethane 80:20) to give **7a** (0.6 g, 1.01 mmol; 78%). M.p. 151 °C; IR (CCl₄): $\tilde{\nu} = 1359$ cm⁻¹ (N–O); UV/Vis (CHCl₃): λ_{\max} (log ϵ) = 300 (4.28, $\pi \rightarrow \pi^*$ aryl-nitroxide), 420 (1.365, $\pi \rightarrow \pi^*$ silole), 448 nm (n → π^* N–O); HRMS (fab+): m/z : calcd for C₃₈H₄₄N₂O₂Si [M+2H]⁺: 588.3172; found 588.3168.

Silole diradical 7b: This compound was prepared starting from compound **6b** in a manner similar to the synthesis of compound **7a** (78%). M.p. 211–213 °C; IR (CCl₄): $\tilde{\nu} = 1354$ cm⁻¹ (N–O); UV/Vis (CHCl₃): λ_{\max} (log ϵ) = 323 (5.351, $\pi \rightarrow \pi^*$ aryl-nitroxide), 400 (5.412, $\pi \rightarrow \pi^*$ silole), 451 nm (n → π^* N–O); HRMS (FAB+): m/z : calcd for C₃₀H₅₂N₂O₂Si [M+2H]⁺: 740.3798; found 740.3787.

Silole diradical 7c: To a suspension of silole **6'** (0.37 g, 0.55 mmol) in diethyl ether (100 mL) was added 0.41 mL (2.57 mmol) of *N,N,N',N'*-tetramethylethylenediamine. The mixture was cooled to –78 °C, and a 2 M solution of *n*-butyllithium in hexane (1.3 mL, 2.57 mmol) was then added under argon. The mixture was stirred for 90 min, warmed to room temperature, stirred for a further 90 min, and then was cooled to 0 °C. A solution of 2-methyl-2-nitrosopropane (340 mg, 3.8 mmol) in diethyl ether (10 mL) was added, and the mixture was stirred overnight at ambient temperature under argon. It was then treated with saturated aqueous ammonium chloride solution (10 mL). The organic layers were combined and concentrated under reduced pressure. Addition of pentane yielded a white precipitate of hydroxylamine that was washed several times with pentane to yield the crude product. The hydroxylamine was sensitive to both moisture and air, so it was used directly to prepare the nitroxide. The white solid was dissolved in freshly distilled dichloromethane (10 mL) and freshly prepared Ag₂O (700 mg, 3 mmol) was added. The mixture was stirred for 60 min at 0 °C, and the solid Ag₂O was removed by filtration. The filtrate was concentrated under reduced pressure and chromatographed (silica gel, ethyl acetate/pentane 3:2) to yield silole **7c** as a reddish orange solid (37%). M.p. 129–132 °C; IR (CCl₄): $\tilde{\nu} = 1357$ cm⁻¹ (N–O); UV/Vis (CHCl₃): λ_{\max} (log ϵ) = 293 (5.304, $\pi \rightarrow \pi^*$ aryl-nitroxide), 363 (5.096, $\pi \rightarrow \pi^*$ silole), 456 nm (n → π^* N–O); HRMS (fab+): m/z : calcd for C₄₆H₄₈N₂O₂Si [M+2H]⁺: 688.3485; found 688.3476.

Silole diradical 7d: This compound was prepared starting from compound **6d** in a manner similar to the synthesis of compound **7a** (78%). M.p. 124–127 °C; IR (CCl₄): $\tilde{\nu} = 1363.2$ cm⁻¹ (N–O); UV/Vis (CHCl₃): λ_{\max} (log ϵ) = 283 (5.31, $\pi \rightarrow \pi^*$ arylaminoxide), 361 nm (5.01, $\pi \rightarrow \pi^*$ silole); HRMS (FAB+): m/z : calcd for C₃₈H₄₅N₂O₂Si [M+3H]⁺: 589.3250; found 589.3251.

***N*-tert-butyl-*N*-(tert-butyl-dimethylsilyloxy)amino-4-phenyl-2-thiophene (8)**: A solution of **4a-TBDMS**^[29] (3.58 g, 0.01 mol) in THF (20 mL) and

[Pd(PPh₃)₄] (0.058 g) were added to a solution of thienylzinc chloride^[30] (0.01 mol) in dry diethyl ether (20 mL). The mixture was then stirred at 50 °C for 16 h, quenched with a saturated NH₄Cl solution and extracted with diethyl ether. The combined extracts were dried over MgSO₄. Evaporation of the solvents and chromatography of the residue (silica gel, pentane) afforded **8** as a white waxy solid (73%). M.p. 56 °C; ¹H NMR (CD₂Cl₂, 298 K): $\delta = -0.02$ (brs, 6H), 0.97 (s, 9H), 1.18 (s, 9H), 7.10 (dd, ¹J(H,H) = 3.4 Hz, ²J(H,H) = 3.6 Hz, 1H), 7.25–7.47 (m, 4H), 7.53 ppm (d, *J*(H,H) = 8.6 Hz, 2H); ¹³C{¹H} NMR (CD₂Cl₂, 298 K): $\delta = -4.50, 18.25, 26.38, 61.31, 122.52, 124.41, 125.96, 131.20, 143.29, 152.18$ ppm; ²⁹Si NMR (CDCl₃, 298 K): $\delta = 23.95$ ppm; IR (KBr): $\tilde{\nu} = 3103, 3070$ (aromatic C–H), 2990–2852 (aliphatic C–H), 1600, 1575 (C=C), 1387 cm⁻¹ (N–O); HRMS (FAB+): m/z : calcd for C₂₀H₃₁NOSSi [M]⁺: 361.1896; found 361.1904.

Bis[*N*-tert-butyl-*N*-(tert-butyl-dimethylsilyloxy)amino-4-phenyl]-2,5-thiophene (9): A 1.33 M solution of *n*BuLi in hexanes (5.3 mL, 7.03 mmol) was added dropwise to a stirred solution of **8** (2.48 g, 6.86 mmol) in diethyl ether (25 mL) at 0 °C. The mixture was stirred for 1 h, and the resulting solution was added to [ZnCl₂(meda)] (1.766 g, 6.99 mmol) dissolved in THF (10 mL) at 0 °C. The mixture was allowed to warm gradually to room temperature to afford the zinc derivative **9** as a light yellow solution. A solution of **4a-TBDMS** (2.45 g, 6.86 mmol) and [Pd(PPh₃)₄] (0.040 g, 35 mmol) in THF (30 mL) was added to the zinc derivative **9** and the reaction mixture was stirred for 18 h at 50 °C. After the usual workup and silica gel chromatography (pentane), **10** was recovered as a white solid (33%). M.p. 130–131 °C; ¹H NMR (CD₂Cl₂, 298 K): $\delta = -0.03$ (s, b, 12H), 0.98 (s, 18H), 1.17 (s, 18H), 7.31 (s, 2H), 7.57 (d, *J*(H,H) = 8.5 Hz, 4H), 7.37 ppm (d, *J*(H,H) = 8.5 Hz, 4H); ¹³C{¹H} NMR (CD₂Cl₂, 298 K): $\delta = -4.49, 18.24, 26.30, 26.35, 61.43, 123.83, 124.67, 126.01, 131.09, 143.29, 151.11$ ppm; ²⁹Si NMR (CD₂Cl₂, 298 K): $\delta = 23.95$ ppm; IR (KBr): $\tilde{\nu} = 3071, 3028$ (aromatic C–H), 2980–2856 (aliphatic C–H), 1600, 1575 (C=C), 1387 cm⁻¹ (N–O); UV/Vis (CHCl₃): λ_{\max} (log ϵ) = 348 nm (4.519, $\pi \rightarrow \pi^*$ thiophene); HRMS (FAB+): m/z : calcd for C₃₆H₅₈N₂O₂Si₂ [M]⁺: 638.3758; found 638.3760.

Bis[*N*-tert-butyl-4-phenylhydroxylamine]-2,5-thiophene (11): A 22.6 M aqueous solution of HF (0.13 mL, 3 mmol) was added to a stirred solution of **10** (0.798 g, 1.25 mmol) in THF (10 mL) at room temperature. After 1 h, the reaction mixture was evaporated under a vacuum to yield the bishydroxylamine as a white solid (99%). M.p. 104 °C (decomp); ¹H NMR ([D₆]DMSO, 298 K): $\delta = 1.14$ (s, 18H), 7.29 (d, *J*(H,H) = 8.5 Hz, 4H), 7.47 (s, 2H), 7.61 (d, *J*(H,H) = 8.5 Hz, 4H), 8.50 ppm (s, b, 2H); ¹³C{¹H} NMR ([D₆]DMSO, 298 K): $\delta = 26.82, 60.91, 125.06, 125.14, 125.47, 130.43, 142.81, 150.76$ ppm; IR (KBr): $\tilde{\nu} = 3230$ (O–H), 3029 (aromatic C–H), 2971–2870 (aliphatic C–H), 1600, 1542 (C=C), 1387 cm⁻¹ (N–O); UV/Vis (CHCl₃): λ_{\max} (log ϵ) = 348 nm (4.519, $\pi \rightarrow \pi^*$ thiophene); HRMS (FAB+): m/z : calcd for C₂₄H₃₀N₂O₂S [M]⁺: 410.2028; found 410.1965; elemental analysis calcd (%) for C₂₄H₃₀N₂O₂S: C 70.21, H 7.36, N 6.82, S 7.81; found: C 70.25, H 7.40, N 6.79, S 7.80.

Bis[*N*-tert-butylaminoxyl-4-phenyl]-2,5-thiophene (12): Further oxidation with PbO₂ (2-fold excess) in dichloromethane at room temperature for 2 h gives a deep red solution that was filtered and evaporated under a vacuum. The resulting deep-red solid was crystallized by diffusion of hexane in dichloromethane to give **12** as black needle-shaped crystals (45%). M.p. 104 °C (decomp); IR (KBr): $\tilde{\nu} = 3069, 3028$ (aromatic C–H), 2997–2853 (aliphatic C–H), 1601, 1580 (C=C), 1349 cm⁻¹ (N–O); λ_{\max} (log ϵ) = 322 (4.167, $\pi \rightarrow \pi^*$ aryl-nitroxide, terphenoquinone), 391 (4.477, $\pi \rightarrow \pi^*$ thiophene), 444 (4.167), 479 (4.072), 551 nm (3.875, $\pi \rightarrow \pi^*$ terphenoquinone); elemental analysis calcd (%) for C₂₄H₂₈N₂O₂S: C 70.56, H 6.91, N 6.86, S 7.85; found: C 70.13, H 7.11, N 6.81, S 7.88. A single crystal of approximate dimensions 0.40 × 0.03 × 0.03 mm³ was mounted on a Nonius κ -CCD diffractometer with MoK α radiation (0.71069 Å) and cooled to 150 K. The diffracted intensities were collected within the range 3.55 < θ < 24.71°. The structural determination by direct methods and the refinement of atomic parameters based on full-matrix least-squares on *F*² were performed with the SHELX-97 programs.^[70] The positions of hydrogen atoms were all calculated. Results: 2[C₂₄H₂₈N₂O₂S]₁: *a* = 20.752(5), *b* = 5.826(5), *c* = 34.309(5) Å, *V* = 4148(4) Å³, ρ_{calcd} = 1.308, system orthorhombic, space group *Pna*2₁, 99.8% completeness to

$\theta = 24.70^\circ$, 24363 collected reflections of which 7020 unique ($R_{\text{int}} = 0.15$) for 523 refined parameters, $R_{\text{obs}} = 0.056$, $wR2_{\text{obs}} = 0.091$, $(\Delta/\sigma)_{\text{max}} = 0.002$, largest max. difference peak and hole 0.40/−0.256 e Å^{−3}.

CCDC-286386 contains the supplementary crystallographic data for **12**. These data can be obtained free of charge from the Cambridge Crystallographic Data Centre via www.ccdc.cam.ac.uk/data_request/cif.

Theoretical calculations: All calculations were performed with the Gaussian 98 package on a Compaq ES40 parallel computer at the Max-Planck-Institut für Bioorganische Chemie.^[34] The UB3LYP exchange-correlation functional and a 6-31G basis set were used for the geometry optimizations owing to the size of the molecules. To obtain accurate spin densities and energies for the calculation of the exchange coupling constant, calculations were then repeated at the minimum geometries with a 6-31+G* basis set, a tight convergence criterion with the limit set to 10^{−8} and the ultrafine integration grid. No spin projection was used in the calculation of the exchange parameter, as advocated by Ruiz et al.^[71] The spin Hamiltonian used to calculate the energy differences was $\hat{H} = -2J\hat{S}_1\hat{S}_2$. The exchange parameter is then obtained as $J = \frac{1}{2}(E_S - E_T)$.

Acknowledgements

This work was supported by the French CNRS and by the European Commission through the Network of Excellence MAGMANet (NMP3/CT/2005/515767). P.G. and N.R. warmly thank Prof. Paul Rey (CEA, Grenoble, France), Prof. Philippe Turek (Institut Charles Sadron, Strasbourg, France), and Prof. Dominique Luneau (Université Claude Bernard-Lyon I, Lyon, France) for their assistance in magnetic characterization and fruitful scientific discussions. We are also indebted to Dr. Bernard Henner (Université Montpellier II, Montpellier, France) for his advice with chemical synthesis. U.S. and E.R. thank Prof. Dr. K. Wieghardt, Max-Planck-Institut für Bioorganische Chemie, Mülheim an der Ruhr (Germany), for access to the computational facilities of the Institute

- [1] S. Nespurek, *J. Non-Cryst. Solids B* **2002**, 299–302, 1033.
- [2] S. Yamaguchi, T. Endo, M. Uchida, T. Izumizawa, K. Furukawa, K. Tamao, *Chem. Eur. J.* **2000**, 6, 1683.
- [3] J. Ohshita, A. Kunai, *Acta Polym.* **1998**, 49, 379.
- [4] M. Ishikawa, J. Ohshita, in *Handbook of Organic Conductive Molecules and Polymers, Vol. 2* (Ed.: H. S. Nalwa), Wiley, New York, **1997**, Chapter 15.
- [5] M. Kira, T. Miyazawa, in *The Chemistry of Organic Silicon Compounds, Vol. 2* (Eds.: Z. Rappoport, Y. Apeloig), Wiley, Chichester, **1998**, p. 1311.
- [6] F. Mercuri, N. Re, A. Sgamellotti, *THEOCHEM* **1999**, 489, 35.
- [7] S. Yamaguchi, K. Tamao, *Bull. Chem. Soc. Jpn.* **1996**, 69, 2327.
- [8] H. Bock, *Angew. Chem.* **1989**, 101, 1659; *Angew. Chem. Int. Ed. Engl.* **1989**, 28, 1627.
- [9] J. Ohshita, H. Kai, T. Sumida, A. Kunai, A. Adachi, K. Sakamaki, K. Okita, *J. Organomet. Chem.* **2002**, 642, 137.
- [10] K. Tamao, M. Uchida, T. Izumizawa, K. Furukawa, S. Yamaguchi, *J. Am. Chem. Soc.* **1996**, 118, 11974.
- [11] S. Yamaguchi, T. Endo, M. Uchida, T. Izumizawa, K. Furukawa, K. Tamao, *Chem. Lett.* **2001**, 98.
- [12] L. Aubouy, P. Gerbier, N. Huby, G. Wantz, L. Vignau, L. Hirsch, J.-M. Janot, *New J. Chem.* **2004**, 28, 1086.
- [13] H. Ago, T. Kuga, T. Yamabe, K. Tanaka, *Chem. Mater.* **1997**, 9, 1159.
- [14] M. Baskett, P. M. Lahti, F. Palacio, *Polyhedron* **2003**, 22, 2363.
- [15] C. Elschenbroich, A. Bretschneider-Hurley, J. Hurley, W. Massa, S. Wocadlo, J. Pebler, *Inorg. Chem.* **1993**, 32, 5421.
- [16] C. Elschenbroich, A. Bretschneider-Hurley, J. Hurley, A. Behrendt, W. Massa, S. Wocadlo, E. Reijerse, *Inorg. Chem.* **1995**, 34, 743.
- [17] Y. Liao, M. Baskett, P. M. Lahti, F. Palacio, *Chem. Commun.* **2002**, 252.
- [18] J. Ohshita, T. Lida, N. Ohta, K. Komaguchi, M. Shiotani, A. Kunai, *Org. Lett.* **2002**, 4, 403.
- [19] N. Roques, P. Gerbier, J.-P. Sutter, P. Guionneau, D. Luneau, C. Guérin, *Organometallics* **2003**, 22, 4833.
- [20] K. Tanaka, H. Ago, T. Yamabe, *Synth. Met.* **1995**, 72, 225.
- [21] Y. Teki, S. Miyamoto, K. Imura, M. Naktsuji, K. Miura, *J. Am. Chem. Soc.* **2000**, 122, 984.
- [22] Y. Teki, S. Miyamoto, M. Naktsuji, Y. Miura, *J. Am. Chem. Soc.* **2001**, 123, 294.
- [23] Y. Teki, *Polyhedron* **2001**, 20, 1163.
- [24] N. Roques, P. Gerbier, S. Nakajima, Y. Teki, C. Guérin, *J. Phys. Chem. Solids* **2004**, 65, 759.
- [25] S. Yamaguchi, K. Tamao, *J. Chem. Soc. Dalton Trans.* **1998**, 3693.
- [26] S. Yamaguchi, K. Tamao, *J. Organomet. Chem.* **2002**, 653, 223.
- [27] E. Negishi, F. T. Luo, R. Frisbee, H. Matsushita, *Heterocycles* **1982**, 18, 117.
- [28] H. Kumagai, Y. Hosokoshi, A. S. Markosyan, K. Inoue, *Polyhedron* **2001**, 20, 1329.
- [29] D. A. Shultz, A. K. Boal, *Mol. Cryst. Liq. Cryst.* **1995**, 272, 297.
- [30] K. Takahashi, T. Suzuki, K. Akiyama, Y. Ikegami, Y. Fukuzawa, *J. Am. Chem. Soc.* **1991**, 113, 4576.
- [31] C. Lee, W. Yang, R. G. Parr, *Phys. Rev. B* **1988**, 37, 785.
- [32] B. Miehlisch, A. Savin, H. Stoll, H. Preuss, *Chem. Phys. Lett.* **1989**, 157, 200.
- [33] A. D. Becke, *J. Chem. Phys.* **1993**, 98, 5648.
- [34] M. J. Frisch, G. W. Trucks, H. B. Schlegel, G. E. Scuseria, M. A. Robb, J. R. Cheeseman, V. G. Zakrzewski, J. A. Montgomery, Jr., R. E. Stratmann, J. C. Burant, S. Dapprich, J. M. Millam, A. D. Daniels, K. N. Kudin, M. C. Strain, O. Farkas, J. Tomasi, V. Barone, M. Cossi, R. Cammi, B. Mennucci, C. Pomelli, C. Adamo, S. Clifford, J. Ochterski, G. A. Petersson, P. Y. Ayala, Q. Cui, K. Morokuma, D. K. Malick, A. D. Rabuck, K. Raghavachari, J. B. Foresman, J. Cioslowski, J. V. Ortiz, A. G. Baboul, B. B. Ste-fanov, G. Liu, A. Liashenko, P. Piskorz, I. Komaromi, R. Gomperts, R. L. Martin, D. J. Fox, T. Keith, M. A. Al-Laham, C. Y. Peng, A. Nanayakkara, M. Challacombe, P. M. W. Gill, B. Johnson, W. Chen, M. W. Wong, J. L. Andres, C. Gonzalez, M. Head-Gordon, E. S. Replogle, and J. A. Pople, Gaussian 98, Gaussian Inc., Pittsburgh PA, **1998**.
- [35] Cambridge Structural Database (CSD), Version 5.27, **2005**.
- [36] P. Pouzet, L. Erdelmeier, D. Ginderow, J.-P. Mornon, P. M. Dansette, D. Mansuy, *J. Heterocycl. Chem.* **1997**, 34.
- [37] W. Schroth, R. Spitzner, C. Bruhn, *Eur. J. Org. Chem.* **1998**, 2365.
- [38] O. Benedi-Borobia, P. Guionneau, H. Heise, F. H. Köhler, L. Du-casse, J. Vidal-Gancedo, J. Veciana, S. Golhen, L. Ouahab, J.-P. Sutter, *Chem. Eur. J.* **2005**, 11, 128.
- [39] D. B. Leznoff, C. Rancurel, J.-P. Sutter, S. J. Rettig, M. Pink, O. Kahn, *Organometallics* **1999**, 18, 5097.
- [40] T. Itoh, K. Matsuda, H. Iwamura, K. Hori, *J. Am. Chem. Soc.* **2000**, 122, 2567.
- [41] S. Nakazono, S. Karasawa, K. Noboru, H. Iwamura, *Angew. Chem.* **1998**, 110, 1645; *Angew. Chem. Int. Ed.* **1998**, 37, 1550.
- [42] K. Takahashi, T. Suzuki, K. Akiyama, Y. Ikegami, Y. Fukuzawa, *J. Am. Chem. Soc.* **1991**, 113, 4576.
- [43] K. Takahashi, A. Gunji, D. Guillaumont, F. Pichierri, S. Nakamura, *Angew. Chem.* **2000**, 112, 3047; *Angew. Chem. Int. Ed.* **2000**, 39, 2925.
- [44] P. M. Lahti, A. S. Ichimura, *J. Org. Chem.* **1991**, 56, 3030.
- [45] A. Calder, A. R. Forrester, S. P. Hepburn, *J. Chem. Soc. Perkin Trans. 1* **1973**, 456.
- [46] A. R. Forrester, R. H. Thomson, G. R. Luckhurst, *J. Chem. Soc. B* **1968**, 1311.
- [47] A. R. Forrester, J. Henderson, S. Hepburn, *J. Chem. Soc. Perkin Trans. 1* **1981**, 1165.
- [48] C. Ling, P. M. Lahti, *J. Am. Chem. Soc.* **1994**, 116, 8784.
- [49] F. Iwahori, K. Inoue, H. Iwamura, *J. Am. Chem. Soc.* **1999**, 121, 7264.
- [50] D. A. O'Brien, D. R. Duling, Y. C. Fann, National Institute of Environmental Health Sciences, National Institutes of Health, USA, WinSim 2002, NT version 0.98, **2002**.

- [51] WINEPR Simfonia, Brucker Ed., 1994–1996, Version 1.25, **1996**.
- [52] W. B. Gleason, R. E. Barnett, *J. Am. Chem. Soc.* **1976**, *98*, 2701.
- [53] B. Bleaney, K. D. Bowers, *Proc. R. Soc. London Ser. A* **1952**, *A214*, 451.
- [54] The magnetic susceptibility measurements were performed at least one week after the isolation of the diradicals.
- [55] O. Kahn, *Molecular Magnetism*, VCH, New York, **1993**.
- [56] T. Matsumoto, T. Ishida, N. Koga, H. Iwamura, *J. Am. Chem. Soc.* **1992**, *114*, 9952.
- [57] U. Schatzschneider, E. Rentschler, *THEOCHEM* **2003**, 638, 163.
- [58] M. Deumal, P. Lafuente, F. Mota, J. J. Novoa, *Synth. Met.* **2001**, *122*, 477.
- [59] C. Rancurel, H. Heise, F. H. Köhler, U. Schatzschneider, E. Rentschler, J. Vidal, J. Veciana, J.-P. Sutter, *J. Phys. Chem. A* **2004**, *108*, 5903.
- [60] P. M. Lahti, M. Minato, C. Ling, *Mol. Cryst. Liq. Cryst.* **1995**, *271*, 147.
- [61] T. Mitsumori, K. Inoue, N. Koga, H. Iwamura, *J. Am. Chem. Soc.* **1995**, *117*, 2467.
- [62] P. M. Lahti, *Magnetic Properties of Organic Materials*, Marcel Dekker, Inc., New York, Basel, **1999**.
- [63] T. Doi, A. S. Ichimura, N. Koga, H. Iwamura, *J. Am. Chem. Soc.* **1993**, *115*, 8928.
- [64] D. A. Shultz, R. M. Fico, Jr., H. Lee, J. W. Kampf, K. Kirschbaum, A. A. Pinkerton, P. D. Boyle, *J. Am. Chem. Soc.* **2003**, *125*, 15426.
- [65] P. R. Serwinski, P. M. Lahti, *Org. Lett.* **2003**, *5*, 2099.
- [66] W. T. Borden, *Diradicals*, Wiley, New York, **1982**.
- [67] D. A. Shultz, R. M. Fico, H. Lee, J. W. Kampf, K. Kirschbaum, A. Pinkerton, P. D. Boyle, *J. Am. Chem. Soc.* **2003**, *125*, 15426.
- [68] M. E. Freeburger, L. Spialter, *J. Org. Chem.* **1970**, *35*, 652.
- [69] G. A. Baker, G. S. Rushbrooke, H. E. Gilbert, *Phys. Rev. A* **1964**, *135*, 1272.
- [70] G. M. Sheldrick, Program for the refinement of crystal structures, University of Göttingen (Germany), Release 97–2 ed., **1998**.
- [71] A. Rodriguez-Fortea, P. Alemany, S. Alvarez, E. Ruiz, *Chem. Eur. J.* **2001**, *7*, 627.

Received: October 14, 2005

Revised: February 8, 2006

Published online: May 8, 2006